UNIVERSITY OF TURIN

UNIVERSITÀ
DI TORINO

Ph.D. Course in Earth Sciences, XXXVI cycle

Ph.D. Thesis

Gypsum twin laws and habits: an unexplored tool as a proxy for the chemistry of the original brine

PhD candidate: Andrea Cotellucci

Supervisor: Prof. Linda Pastero

A.A. 2020-2023

The candidate confirms that the work submitted is his own. The contributions of the candidate and the other authors to this work have been explicitly indicated overleaf. The candidate confirms that appropriate credit has been given where reference has been made to the work of others.

Abstract

Identifying the impurities that promote the selection of specific twin laws of gypsum has relevant implications for the geological studies aimed at interpreting the gypsum depositional environments both in ancient and modern deposits. However, because of the limited knowledge of morphological, crystallographic, and optical characteristics of the five twin laws of gypsum, relatively little has been done to understand which impurities exert a critical role in the selection of different twin laws and how this may impact our awareness about their occurrence in nature. Typically, the 100 contact twin law has been the only twin law of gypsum known so far in nature. Still, some sedimentological-stratigraphic studies suggested this might not be the only widespread one. In this thesis, we firstly provided a geometric-crystallographic background of the five twin laws of gypsum, allowing researchers to recognize the twin laws only by the measurement of i) their re-entrant angle value and ii) the extinction angle formed between the two individuals using crossed polarizers in optical microscopy. Moreover, we designed specific crystal growth laboratory experiments to improve our understanding of different habits and twin laws of gypsum occurring i) in a pure system; ii) with and without the addition of carbonate ions in solution; iii) in the presence and absence of sulfide oxidation. The main results suggest that the crystal aspect ratio (length/width crystal ratio), the different orientation of primary fluid inclusions with respect to the twin plane, and the main elongation of the sub-crystals making the twin, should be a useful tool to distinguish between 100 and $\overline{1}01$ twin laws, whose geometry is otherwise very hard to distinguish, especially in rock samples. Moreover, gypsum twins obtained by crystal growth laboratory experiments are compared with those detected in natural environments and i) the occurrence of the $\overline{1}01$ twin law is suggested occurring in evaporitic-sedimentary environments; ii) the overall chemical species resulting from H_2S oxidation in solution may be involved in triggering the precipitation of 100 contact twins during the Messinian Salinity Crisis.

The results presented in this thesis i) describe which among the twin laws of gypsum are possible in a pure solution and, for the first time, establish a correlation between different gypsum habits and evaporation rates, so contributing to a better understanding of gypsum growth morphology in evaporitic environments; ii) provide new insights into the mineralogical implications of twinned gypsum crystals and their potential use as a tool for a deeper comprehension of the natural gypsum deposits; iii) may contribute to the debate on the origin of ancient Salt giants, where 100 gypsum contact twins constitute a typical mineral component, providing new experimental data and stimulating further research in the field of the sulfur cycle in sedimentary environments.

Thesis outline and declarations

This work consists of five chapters:

- **Chapter 1** firstly introduces only the crystal growth basic concepts required to understand the results described in the manuscript. A complete treatment about crystallography and crystal growth principles can be found in the excellent textbooks by Mutaftschiev, 2001; Rigault, 2005; Dhanaraj et al., 2010. Moreover, it also provides an overview of the literature i) on the equilibrium habit of gypsum crystals; ii) on the effects of solution chemistry on the crystal growth habit; and iii) suggests a reason why the study of twinned gypsum crystals has been a challenging task in recent decades and describes the contribution of this manuscript to the topic.
- **Chapter 2** contains a brief geometric-crystallographic description of the five twin laws of gypsum and their identification by means of optical microscopy. Moreover, it shows which single and twinned habits of gypsum arise from the evaporation of a pure solution, relating them to different evaporation rates. The first part of Chapter 2 ("*Geometric-crystallographic background to identify the different gypsum twin laws and habits*") reproduces a paragraph of a peer-reviewed publication in *J. Appl. Cryst.* (Cotellucci et al., 2023a), whereas the second part of the chapter is a reproduction of a peer-reviewed publication in *Cryst. Growth Des.* (Cotellucci et al., 2023b).
- In **chapter 3** the effect of calcium carbonate ($CaCO_3$) on gypsum ($CaSO_4 \cdot 2H_2O$) growth morphology is described by performing temperature-controlled laboratory experiments with and without adding carbonate ions. This chapter is a reproduction of a peer-reviewed publication in *J. Appl. Cryst.* (Cotellucci et al., 2023a).

- **Chapter 4** presents a basic setup to precipitate gypsum from mixing of gaseous H_2S and $Ca(OH)_2$ solution and by evaporating a Ca^{2+}-SO_4^{2-} rich solution.
- Finally, in **chapter 5**, concluding remarks, and a summary of the results described in previous chapters, are reported.

CONTENTS

Chapter 1

Introduction

1.1. Background information

1.1.1. Gypsum structure

Gypsum (calcium sulfate dihydrate, $CaSO_4 \cdot 2H_2O$) belongs to the sulfate mineral class (Dana, 1864) and it is characterized by the presence of the sulfate group (SO_4^{2-}), where sulfur coordinates four oxygen atoms located at the vertices of a tetrahedron. The structure of gypsum, firstly determined by Wooster (1936), is composed by layers of SO_4 – Ca – SO_4 with double sheets of sulfate groups, separated by water molecules on the 010 crystal planes. The alternation of the different layers occurs along [010], and each calcium ion is coordinated by eight oxygens atoms: six belonging to SO_4 tetrahedra and two to water molecules (Fig. 1). Moreover, water molecules are linked to the sulfate layers by hydrogen bonding, which has a relatively weak energy and thus is responsible for the perfect {010} cleavage of gypsum (Styles et al., 1996).

The repetition of gypsum's structure in three dimensions follows that of the monoclinic system, however the assignment of the unit cell is not univocal. In the gypsum structure, the [010] (≡b axis) is determined by identifying the second-order rotation (C_2 symmetry operation) whereas in the xz plane (≡ (010) plane) the unit cell can be described by different nearly equivalent vectors. Consequently, gypsum was historically indexed in a variety of ways (e.g., Cole and Lancucki, 1974; Pedersen and Semmingsen, 1982; Boeyens and Ichharam, 2002). These different choices are a potential source of confusion and mistakes, as the indexing of crystallographic planes and directions changes with the reference frame chosen. Hence, the reference frame used must always be reported. A comparison of these indexing possibilities has been presented by Massaro et al. (2010) and by Aquilano et al. (2016) (Appendix A; Fig. S1 and Table S1). For the sake of clarity, in this manuscript we adopt the monoclinic *C2/c* space

group where $a_0 = 5.63$, $b_0 = 15.15$, $c_0 = 6.23$ Å; $\alpha = \gamma = 90°$; $\beta = 113.50°$ (de Jong and Bouman, 1939). Our choice is grounded on two practical reasons:

I. This frame uses the smallest lattice vectors.

II. The [001] ≡ z axis coincides with the morphological elongation of the crystals growing from pure aqueous solution and most natural crystals.

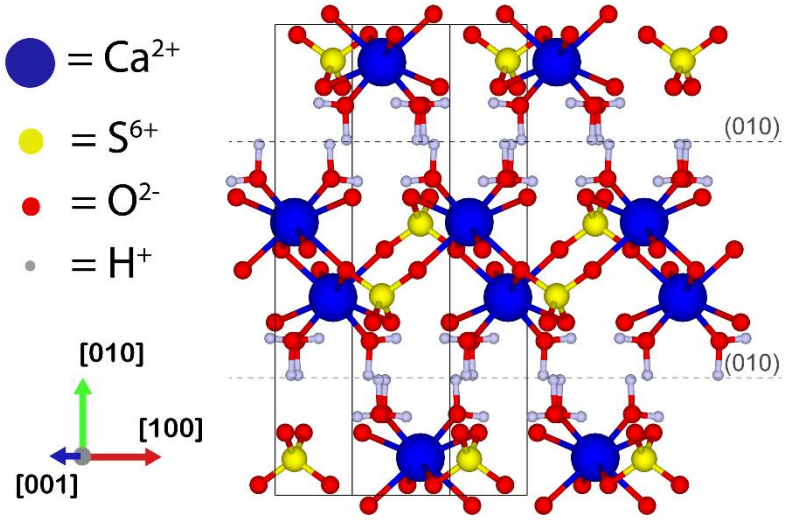

Figure 1 Structure of gypsum projected along the [001]* reciprocal axis.

1.1.2. Crystal forms

Starting from the mother phase (vapor, solution, or melt), nuclei grow developing faces, which define the habit of the stable crystals. From a crystallographic point of view, a face is identified by its Miller indices (*hkl*). The set of all (*hkl*) faces which can be generated by the point group operations, is a crystal form {*hkl*} that is geometrically represented by a polyhedron (Fig. 2); e.g., the six faces of a cube, (100), (010), (001), ($\bar{1}$00), (0$\bar{1}$0) and (00$\bar{1}$), belong to the crystal form {100}. Depending on the number of equivalent (*hkl*) faces (imposed by the multiplicity of the point group, depending of the general or special nature of the form) and elements of symmetry involved (e.g., inversion center, rotation of 180°, mirror plane), the polyhedrons of different crystal forms {*hkl*} are defined by a specific name (Rigault, 2005). Which among these forms will be displayed in the equilibrium shape of the crystal is defined by the Gibb-

Wulff theorem, where the convex polygon made by crystal forms with the lowest surface energies γ_j are those exploited to compose the crystal equilibrium shape (Mutaftschiev, 2001; Dhanaraj et al., 2010).

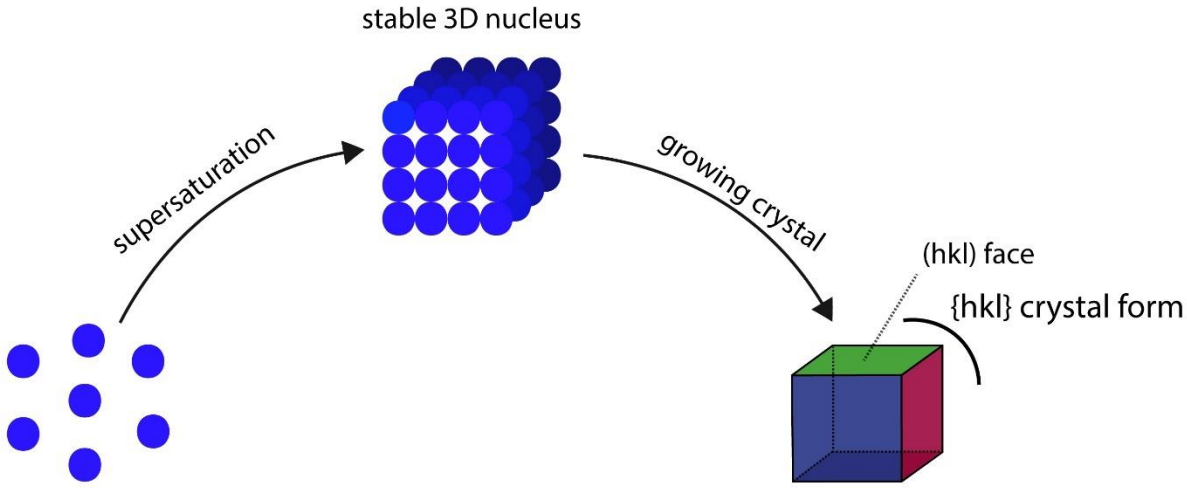

Figure 2 Schematic representation of the formation of a 3D nucleus showing its {*hkl*} crystal forms.

1.1.3. Periodic Bond Chain theory coupled with computational methods: a methodological approach to calculate surface energies

A Periodic Bond Chain (PBC), firstly introduced by Hartman and Perdok (Hartman and Perdok, 1955a, 1955b, 1955c), is an uninterrupted periodic chain of strong bonds between the growth units (ions, molecules) running along the crystallographic directions defined as [*uvw*]. Such directions determine the character of the {*hkl*} crystal forms, influencing in this way the morphology of a crystal (Hartman and Perdok, 1955b). Once the PBC's are found after examination of the crystal structure, the faces can be classified into three types: F, S, and K (Fig. 3). When at least two non-parallel PBCs run within a d_{hkl} thickness allowed by the space group of the crystal (d_{hkl} represents the interplanar spacing for a family of planes with Miller indices *hkl*), the related {*hkl*} crystal form has a F (Flat) character. This means that the faces are flat, growing by lateral extension of growth layers, and their growth rate is low.

Consequently, they have a real chance to appear on the final crystal habit. If only a PBC runs within a d_{hkl} thickness, the $\{hkl\}$ crystal forms have an S (Stepped) character, i.e., each step develops independently of the parallel neighboring steps. They grow faster than F crystal forms and normally do not appear on the growth form unless, as we will see later, they are stabilized by impurities. Finally, when no PBC are found, K (kinked) character, the $\{hkl\}$ crystal forms are energetically and kinetically unstable. The growth rate of a K-form is so high that normally it does not occur on the crystal habit and, when it appears, its existence results either from a high supersaturation or from an impurity effect.

Once the F, S and K face characters are defined, empirical, semi-empirical, quantum-mechanical, or molecular dynamics calculations can be performed. These approaches allow us to thoroughly analyze and classify the intermolecular interactions together with the character of crystal faces according to the PBC theory, with the final aim of calculating their specific surface energies γ_j eventually leading to the prediction of the equilibrium crystal habit (e.g., Aquilano et al., 1997; Bruno et al., 2013; Sun et al., 2015).

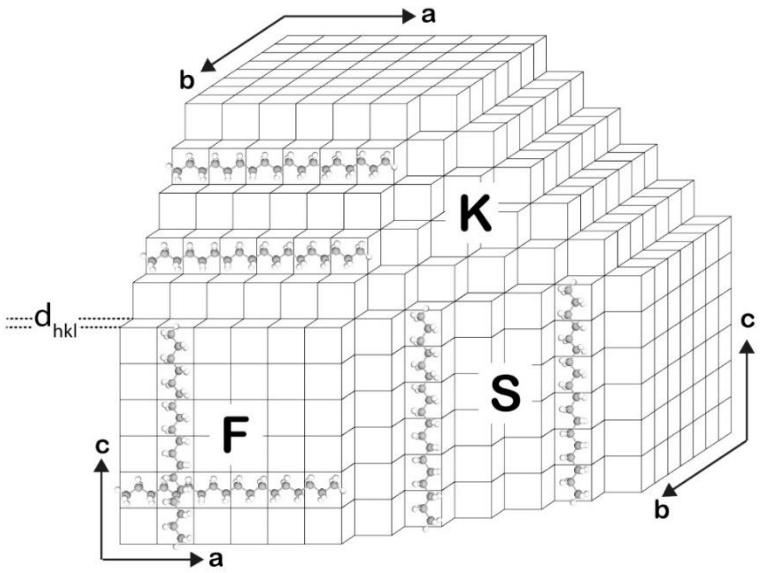

Figure 3 Schematic representation of a crystal. Depending on the number of PBCs occurring within the slice d_{hkl}, the related $\{hkl\}$ crystal form can exhibit a F (flat), S (stepped), or K (kinked) character.

1.2. Equilibrium and growth habit of gypsum: the significance of the on-field-experimental data to improve theoretical models

The equilibrium crystal shape (ES, hereinafter), generally called "equilibrium habit", is defined for a crystal in equilibrium with its mother phase (Dhanaraj et al., 2010). Applied to computational methods, this means in vacuum or solvent medium depending on whether the computational methods used are complex enough to consider the solid-solvent interaction when calculating the specific surface energies γ_j (Massaro et al., 2011; Sun et al., 2015; Khalkhali et al., 2019). In nature, and mostly in crystal growth laboratory experiments, the equilibrium is rarely achieved because a closed system or long equilibrium time are required to reach the equilibrium shape. An example of crystals showing an equilibrium habit are those found in the geological so-called "geodes" which represent a naturally occurring closed system, whereas long crystallization geological times in an open system are supposed for meter-sized gypsum crystals found in Naica (Mexico) (García-Ruiz et al., 2007; Otálora and García-Ruiz, 2014). All crystals not satisfying these crystallization conditions (overall crystals synthesized through laboratory experiments) are defined with a growth habit, i.e., the crystal may show energetically unstable crystallographic forms (Stepped or Kink forms) along with the stable ones (Flat forms).

The first prediction of ES of gypsum goes back up to '60s. Simon and Bienfait (1965) predicted a platy ES, dominated by the {010} pinacoid, the {120} prism and {011} prism but, as they themselves recognized, their ES was very different from the experimental habit (Simon, 1968) (Fig.4A vs 4C). The disagreement was related to the limitations of the computational method used to calculate the crystal surface energies γ_j (Aquilano et al., 2016), where:

I. The crystal was assumed to be in vacuum, thus solvent interactions were not considered.

II. Relaxed interfaces were not considered: atoms and molecules were approximated as rigidly fixed points in their crystallographic positions in the crystal bulk.

III. Only for the theoretically most stable crystallographic forms (Flat forms) surface energies γ_j were calculated.

IV. Extinction rules were not considered in the selection of the candidate forms, and as a consequence, higher order families of equidistance (i.e., $d_{hkl}/2$, $d_{hkl}/3$, $d_{hkl}/4$,…) were not taken into account.

After the pioneering work by Simon, many other authors dealt with gypsum modeling, always improving the computational methods used (e.g., Weijnen et al., 1987; van der Voort and Hartman, 1991; Heijnen and Hartman, 1991). Up to the 2000s the ES determined by Heijnen and Hartman (1991) (Fig. 4D) was used as a references among researcher dealing with gypsum habit investigation because it was the closest to the experimental one (Rodríguez-Blanco et al., 2007; Pinto et al., 2010; Van Driessche et al., 2010). However, in this period an important discovery was made. Giant gypsum crystals (up to 11 meter long and 1 meter thick) were discovered in the Naica mine (Mexico), in the so-called *Cuevas de los Cristales*. These crystals are supposed to have grown from an anhydrite-gypsum thermally driven transformation by a self-feeding mechanism at very low supersaturated solutions, and over a very long time. To date, their crystal habit is considered as the best natural approximation of the ES of gypsum (García-Ruiz et al., 2007; Otálora and García-Ruiz, 2014). The single crystal habit is described as blocky and prismatic, defined by huge {1k0} prisms, {010} pinacoid, and capped by $\{\bar{1}11\}$ prism with the {011} form only marginally present (Fig. 4B). The {1k0} prisms are composed by the {120}, {140} and {160} crystal forms, and the most extended one is the {140} instead of the {120} (García-Ruiz et al., 2007; Otálora and García-Ruiz, 2014). This extraordinary discovery revealed how deep were the discrepancies of theoretical modeling compared to the evidence. These contradictions stimulated the researchers to perform more accurate computational calculations than previously known, to bring together theoretical equilibrium habit with that observed in *la Cueva de los Cristales*. Aquilano and coworkers re-examined the

ES of gypsum, finding that a more accurate model for the crystal surface explained all these features (Massaro et al., 2010, 2011; Rubbo et al., 2011). Using energy minimization methods and considering surface relaxation, these authors showed that the re-orientation of water molecules modifies their coordination and the number of unsaturated bonds exposed. The resulting ES is dominated by four F forms, {010}, {120}, {011} and {$\bar{1}$11} and smoothed by four S forms, {100}, {$\bar{1}$22}, {140}, {180}, demonstrating that the contribution of the surface relaxation and water-crystal surface interaction are not negligible (Aquilano et al., 2016) (Fig. 4E).

Thanks to this accurate modeling, at the present is proved that blocky gypsum crystals found in *la Cuevas de los Cristales* are the best natural representation about the ES of gypsum crystals.

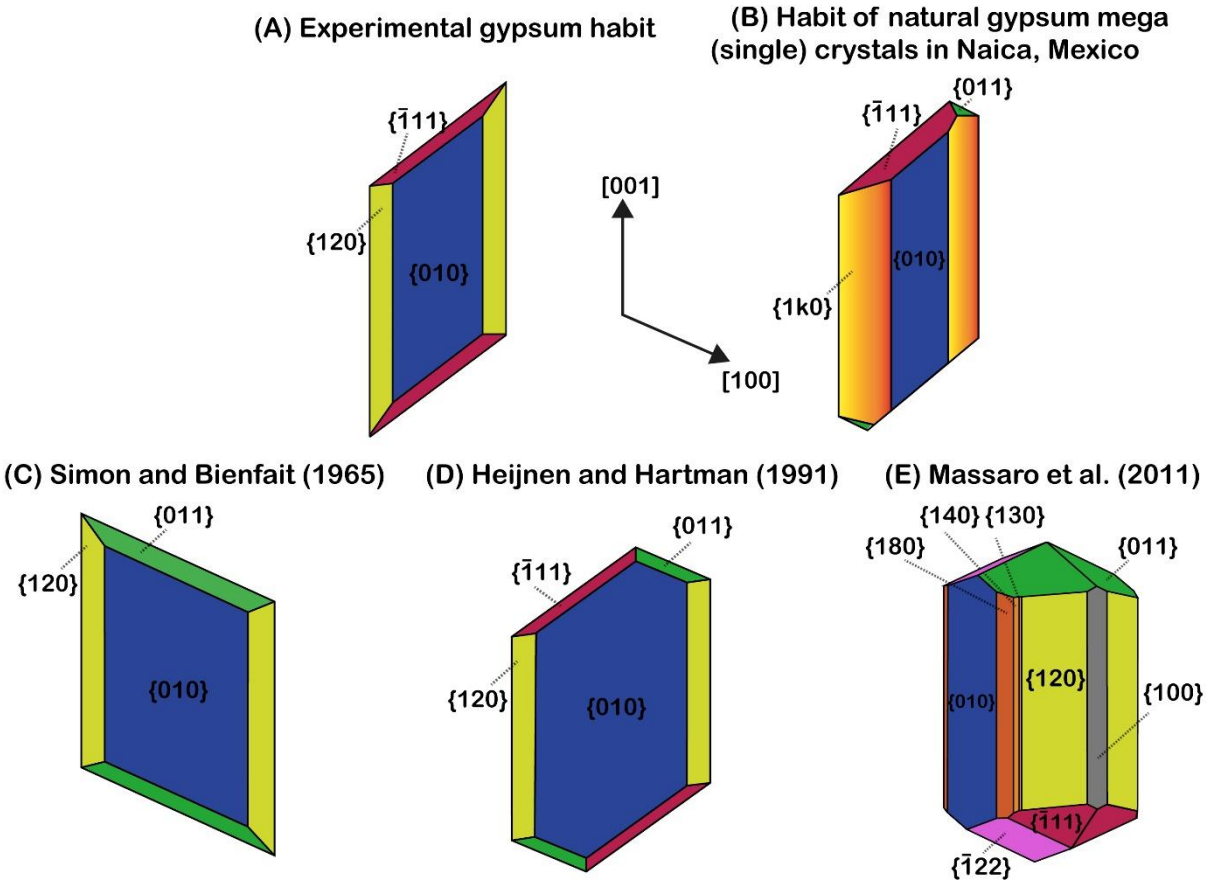

Figure 4 A-B) Geometry of the most common gypsum single crystal habits detected by (A) crystal growth laboratory experiment and (B) in *la Cueva de los Cristales*, Naica (Mexico). C-E) Selection of the equilibrium morphologies for gypsum, from literature.

1.3. Different gypsum crystal habits: the main chemical and physical factors responsible for the morphological variability

Since the pioneering studies of Lacroix (1893), the different habits of gypsum were believed to reflect peculiar growth conditions. A better understanding of the environmental factors responsible for different gypsum crystal habits may have crucial implications for the interpretation of the origin of the gypsum deposits formed in the geological past. Moreover, precise control over the habit of gypsum are of tremendous interest in industrial applications, where gypsum often precipitates forming undesired deposits having potential negative economic effects on desalination processes (Rosenberg et al., 2012; Reiss et al., 2021; Ramírez-García et al., 2022).

Depending on the depositional environment, gypsum exhibits different idiomorphic single and twinned crystal habits. In soils (Jafarzadeh and Burnham, 1992), desert regions (Shahid and Abdelfattah, 2009) and salt lakes (Warren, 1982; Mees et al., 2012), acicular, tabular-prismatic, lenticular, and twinned crystals are observed. In marine evaporites, mostly twinned and tabular gypsum crystals are found (Ortí, 2010); in caves and in Badenian evaporitic gypsum deposits, distinctive curved crystal structures (the so-called ram's horn and sabre gypsum) are observed (Wenrich and Sutphin, 1994; Panczner, 1987; Bąbel et al., 2015), whereas the most spectacular habits are related to the prismatic meter-sized single crystals and twins of Naica Mine (Mexico) (García-Ruiz et al., 2007; Otálora and García-Ruiz, 2014) and in the Geode of Pulpì (Almería, Spain) (Canals et al., 2019), which grew by an anhydrite-gypsum thermally driven transformation by a self-feeding mechanism at low supersaturation values (Fig 5).

The acicular habit developed along [001] is the most common and representative of gypsum habit in a pure system (e.g., Craker and Schiller, 1962; Rinaudo et al., 1985; Montagnino et al., 2011), whereas tabular-prismatic and lenticular habits are promoted by different growth conditions, overall, Ca^{2+}/SO_4^{2-} ratio (Mbogoro et al., 2017; Reiss et al., 2019), and chemical

composition of the mother solution (e.g., Cody, 1979; Rabizadeh et al., 2017; Reiss et al., 2021). These variables affect the mechanisms governing the growth of crystal faces (Van Driessche et al., 2011; Mbogoro et al., 2017; Van Driessche et al., 2019; Criado-Reyes et al., 2020), and hence, the final habit that crystals show. Twinning is an epitaxial phenomenon that involves a regular mutual orientation between two (or more) individuals of the same crystal phase: the Parent (P) and Twinned (T) crystals (Bruno et al., 2022a). Twinned crystals are the result of the so called "twin operation" (e.g., mirror plane, inversion center), of the crystal structure with respect to a specific plane: the twin law (Parsons, 2003). Twinning occurs under condition of supersaturation, where a crystallization unit (an atom or group of atoms) takes an energy such that a second individual is generated, twinned with respect to the original crystal. This crystallization unit can be temporarily blocked by subsequent deposition units and then proceeds to grow, resulting in a second twinned crystal. In terms of their genesis, gypsum twins are categorized as *growth twins,* formed during the crystal growth process. Other categories for twins in any inorganic crystal structure include *transformation twins,* formed following a phase transition, where symmetry elements lost in the transition act as twin elements, and *mechanical or gliding twins,* which result from structural shear in plastic deformation. Both the oriented attachment and classical nucleation mechanisms for the formation of *growth twins* have been described (Nespolo and Ferraris, 2004). However, experiments are lacking up to date, aimed at elucidating whether the oriented attachment or the classical nucleation mechanisms are involved in the formation of gypsum twins. Five different twin laws are possible for gypsum (Follner et al., 2002) and each twin law is described by a contact and a penetration twin (Rubbo et al., 2012a, 2012b), hence, at least ten different twinned habits are possible.

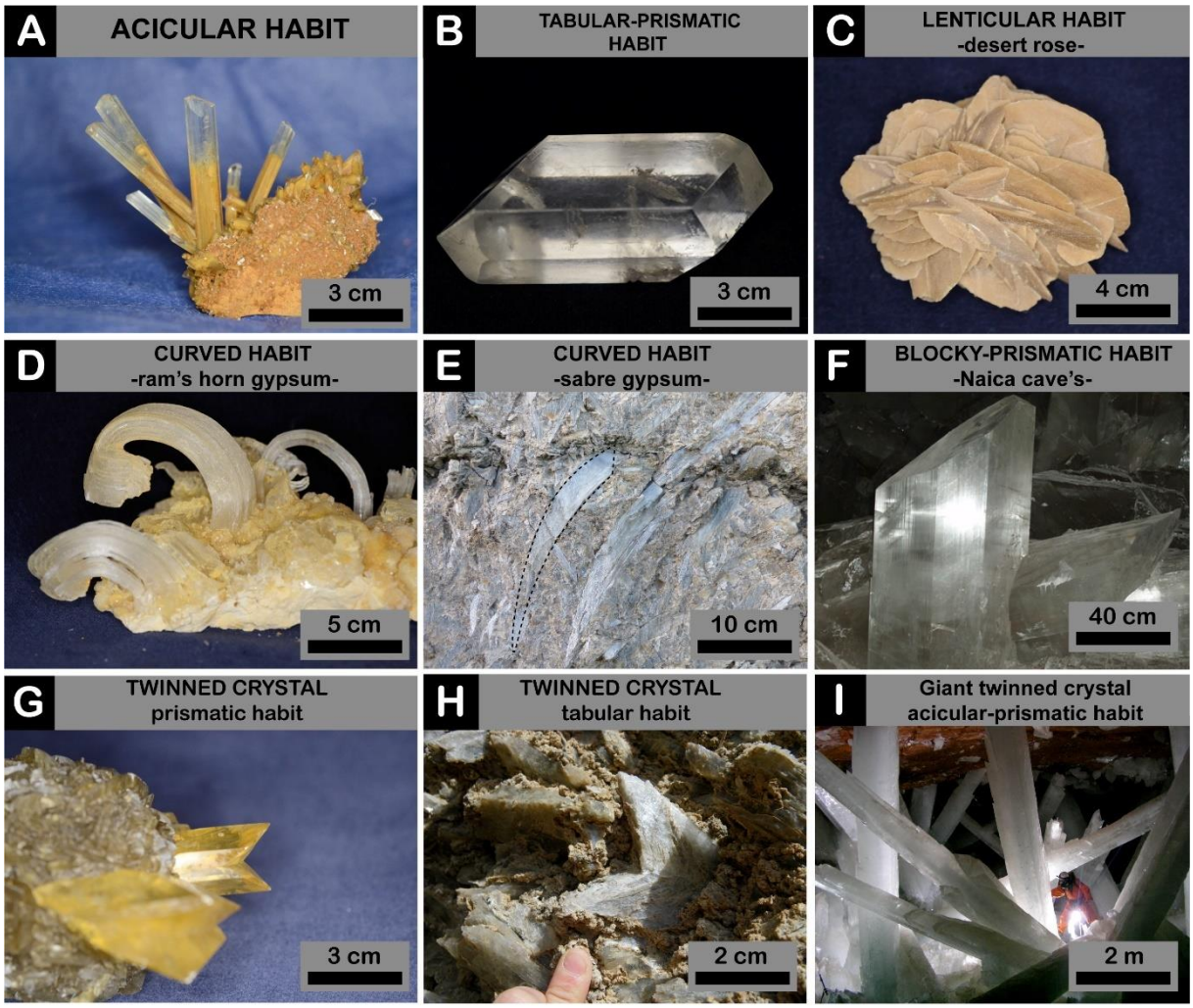

Figure 5 A) Acicular habit from Mexico, Naica (collection of the Turin Natural Science Regional Museum). B) Tabular-prismatic habit from Canada, Alberta, Chaine Lake (collection of the Turin Natural Science Regional Museum). C) Lenticular crystals aggregated together to form the well-known "desert rose" (from Tunisia; collection of the Turin Natural Science Regional Museum). D) Ram's horn gypsum from Sicily, Cava di Rocca Chi Parra (collection of the Turin Natural Science Regional Museum). E) Curved gypsum crystals (sabre gypsum) from the Badenian succession of Poland F) Blocky-prismatic single crystal from Mexico, Naica (ph. Juan-Manuel Garcia-Ruiz). G) Prismatic twinned crystal from Red River Floodway, Winnipeg, Manitoba, Canada, (collection of the Turin Natural Science Regional Museum). H) Prismatic twinned crystal from Spain, Sorbas (ph. Laura Sanna). I) Giant acicular-prismatic twinned crystals from Mexico, Naica (ph. Laura Sanna - LaVenta archive).

1.3.1. Calcium-sulfate ratio

Each gypsum crystal form ($\{hkl\}$) is defined by a surface structure and then by a specific surface energy, consequently each crystal form has its own reactivity toward the mother phase. It follows that some crystal forms grow faster than others and this different reactivity could change whether "external" factors change as well. Ca^{2+}:SO_4^{2-} ratio is one of those factors affecting gypsum kinetics, and thus, the habit (Mbogoro et al., 2017; Reiss et al., 2019); the exceeding counterion plays the role of a surface specific impurity in the system. At constant supersaturation, and only by mixing $CaCl_2 \cdot 2H_2O$ together with Na_2SO_4 at different relative concentrations, Ca^{2+}:SO_4^{2-} ratio (r= Ca^{2+}:SO_4^{2-} ratio, hereinafter) influences the rate of growth of the main crystal faces of gypsum. The acicular habit developed along [001] has been observed for r>1, whereas a tabular habit developed toward both [001] and [100] has been described for r<<1 (Mbogoro et al., 2017). Further information is provided by Reiss et al. (2019), who dealt with the investigation of the gypsum habit at constant supersaturation, varying Ca^{2+}:SO_4^{2-} ratio and reproducing solution chemistry close to its natural evaporitic counterpart (i.e., r>>1, ionic strength>3 and with a broad range of inorganic background electrolytes dissolved in solution). They observed that low *r* values produce acicular habits whereas high *r* values tabular habits. These results are at the opposite with respect those reported by Mbogoro et al. (2017), however, we must recognize that the different results provided by the two authors are not comparable because of the different growth conditions investigated: in Reiss et al. (2019) the experimental growth conditions are specific for evaporitic environments, and thus, the cooperative effect among inorganic additives dissolved in solution, along with different Ca^{2+}:SO_4^{2-} ratio and high ionic strength, could have modified the reactivity of crystal forms of gypsum toward the mother solution with respect to simpler growth conditions performed by Mbogoro et al. (2017).

To summarize, Ca^{2+}:SO_4^{2-} ratio influences the habit of gypsum crystals and, in the simplest growth conditions, r>1 produce acicular habit whereas r<1 tabular one. However, more complicated growth conditions can promote a different reactivity of gypsum crystal forms toward the mother solution and completely reverse this trend.

1.3.2. The effect of inorganic and organic additives as efficient habit modifier's

Many crystal growth experiments have been performed to establish which conditions favor gypsum habits. Acicular gypsum single crystals were observed i) in a gel medium (Rinaudo et al., 1985), ii) from the hydration of bassanite (Craker and Schiller, 1962), iii) by evaporation of $Ca^{2+} - SO_4^{2-}$ rich water solutions at 35°C (Montagnino et al., 2011), just to name a few. Reiss et al. (2019) observed that saline water with Na^+, K^+, Mg^{2+}, Sr^{2+}, Cl^-, Br^- ions in solution reduce the [001] elongation of gypsum single crystals switching from acicular to tabular habit, and Rabizadeh et al. (2017) demonstrated that Na^+, K^+, Li^+, and Mg^{2+} ions affect the nucleation, growth kinetics and habit of gypsum. Na^+ ions are incorporated into the synthesized crystals, whereas K^+, Li^+, and Mg^{2+} ions are only adsorbed on the surfaces. Organic molecules from green plants' decomposition promote the lenticular habit (Cody, 1979). Moreover, specific additives have been used to modify the precipitating morphology of gypsum in desalination pipelines to prevent them from adhering to the surface of apparatuses. One of the most important and widely used groups of antiscalant (also called scale inhibitors) is phosphonic acid derivates. Such antiscalant have phosphonates as functional group which have been reported as efficient inhibitor for gypsum (e.g., Akyol et al., 2009; Reiss et al., 2020; Prisciandaro et al., 2022). These additives promote the precipitation of less elongated gypsum crystals with respect to those precipitated in a pure solution (Akyol et al., 2009; Rabizadeh et al., 2020). Such morphological modification has been interpreted as due to the negative functional group that forms complexes with Ca^{2+} ions exposed onto crystal surfaces (affecting the crystallization and morphology of precipitating crystals (Akyol et al., 2009; Rosenberg et al., 2012)), or

incorporated into the synthesized crystals (Rabizadeh et al., 2020), hence preventing crystal growth. However, despite their high capacity as antiscalant agents, phosphonate additives are environmental "unfriendly" because they would cause eutrophication if used in large amounts (Ramírez-García et al., 2022). To face this problem, "green", biodegradable polymers have received increasing interest as a potential substitute of phosphonate additives for water treatment during scale inhibition (e.g., Popov et al., 2016; Rabizadeh et al., 2019; Ziegenheim et al., 2021). To the best of our knowledge, poly-carboxylic acids are the most tested and promising bio-molecules (e.g., Ziegenheim et al., 2021; Ramírez-García et al., 2022). However, we envisage that the increasing necessity to find always more and more green and efficient scale inhibitors will bring researchers to expand the type of (bio)molecules tested.

Despite their variability, only two twin laws of gypsum have been observed, both in natural and laboratory environment and, occasionally, the identification of the twin laws has been debated. Kern and Rehn (1960), as well as Simon (1968), argued that both 100 and $\bar{1}01$ penetration twin laws of gypsum are usual in pure aqueous solution, with the $\bar{1}01$ penetration twin law being the more prevalent of the two, whereas Cody and Cody (1989a) concluded that the $\bar{1}01$ penetration twin law recognized in previous works (Kern and Rehn, 1960; Simon, 1968) were 100 twins instead. On the other hand, it is widely accepted that α-amylase triggers the precipitation of a peculiar gypsum twin habit similar to those present in the Eocene deposits of the Paris Basin, the so-called Montmartre twin (Cody and Cody, 1989b; Van Driessche et al., 2019), and the 100 contact twin law is the most widespread twin law in natural environments (Ortí, 2010; Otálora and García-Ruiz, 2014).

1.4 Research objectives and main results

Even though gypsum has been studied for more than one century, only a limited number of works focused on gypsum twins. A limited knowledge of the morphological, crystallographic, and optical characteristics of the five twin laws of gypsum may be at the origin of this gap. This

would explain i) why the twin laws of gypsum in a pure solution are still debated; ii) why "swallowtail twin" is the terminology usually used to identify gypsum twinned crystals with a shape at a first glance similar, avoiding the twin law identification.

To improve our awareness about the occurrence of different twin laws and habits of gypsum both in natural and laboratory environments, it is required to define i) the main structural-crystallographic characteristics which differentiate twin laws; ii) some easy and practical tools for univocally identifying the twin laws. Hence, in these three years of investigation we tried to fill this gap in knowledge. After a short, but useful, geometric-crystallographic description of the five twin laws of gypsum and their identification by means of the optical microscopy, we show specific crystal growth laboratory experiments designed to improve our understanding of different habits and twin laws occurring i) in a pure system (chapter 2), ii) with and without calcium carbonate dissolved in solution (chapter 3), iii) in the presence and absence of H_2S oxidation (chapter 4). Starting from solutions saturated in $CaSO_4{\cdot}2H_2O$ and allowing them to evaporate at different evaporation rates (chapter 2), we correlated different gypsum habits to the evaporation rates, contributing to a better understanding of gypsum habits in evaporitic environments. In chapter 3, the effect of carbonate ions triggering the formation of $\overline{1}01$ gypsum contact twins is described. An epitaxial mechanism between the (100) face of rapidcreekite ($Ca_2SO_4CO_3{\cdot}4H_2O$) and the (010) face of gypsum ($CaSO_4{\cdot}2H_2O$) is suggested to explain the $\overline{1}01$ gypsum contact twin formation. Moreover, we compared the natural gypsum twin morphologies observed in evaporitic environments with those obtained in our experiments and suggested the occurrence of $\overline{1}01$ gypsum contact twins in nature. We claim that the occurrence of $\overline{1}01$ gypsum contact twins in nature is probably more widespread than believed, and it might be an indicator of high carbonate concentration in brine from which they precipitated. Finally, it has been shown that the different orientation of primary fluid inclusions (of the negative crystal-shaped) with respect to the twin plane, and the main elongation of the sub-crystals

making the twin, are useful tools to distinguish between 100 and $\bar{1}01$ twin laws, whose geometry is otherwise very hard to distinguish especially in rock samples.

Finally, chapter 4 analyzes the different gypsum habits observed both in presence and absence of sulfide oxidation. The preliminary results suggest that H_2S, along with its oxidation products, may promote the precipitation of 100 gypsum contact twin, and the possible geological implications of these laboratory experiments are discussed.

Chapter 2

The effect of different evaporation rates on gypsum habit: mineralogical implications for natural gypsum deposits

2.1. Introduction

To recognize the effect of impurities on gypsum habit, the impurity-free gypsum habit must be known. This has been often obtained in the literature by mixing calcium chloride dihydrate ($CaCl_2 \cdot 2H_2O$) or calcium nitrate ($Ca(NO_3)_2$) with sodium sulfate (Na_2SO_4) to produce supersaturated solutions with respect to calcium sulfate dihydrate ($CaSO_4 \cdot 2H_2O$) (Budz et al., 1986; Cody and Cody, 1989b; De Vreugd et al., 1994). This approach mostly produces acicular crystals (Morales et al., 2016; Rabizadeh et al., 2014). Unfortunately, Na^+ ions affect the nucleation, growth kinetic and habit of gypsum crystals, and are structurally incorporated into the crystals through the substitution of Na^+ for Ca^{2+} ions because of the closest ionic radius of Na^+ (1.16 Å) to Ca^{2+} (1.12 Å) (Rabizadeh et al., 2017). Therefore, this synthesis does not reflect the habit of gypsum grown in a pure system, since it contains sodium chloride or nitrate coming from reagents.

As already mentioned in chapter 1, other experiments have been designed to obtain gypsum crystals from a pure solution including: a) the hydration of bassanite (Kern and Rehn, 1960), and b) the evaporation of a solution saturated in $CaSO_4 \cdot 2H_2O$ (Simon, 1968; Cody and Cody, 1989b). In these experiments, twinned crystals have been commonly detected. However, the identification of their twin laws has been debated (Cody and Cody, 1989b) because of the limited knowledge of the morphological, crystallographic, and optical characteristics of the five twin laws of gypsum. Kern and Rehn (1960), as well as Simon (1968), argued that both 100 and $\bar{1}01$ penetration twin laws of gypsum are usual in pure aqueous solution, with the $\bar{1}01$ penetration twin law being the more prevalent of the two. On the opposite, Cody and Cody,

(1989b) concluded that the $\bar{1}01$ penetration twin law, recognized in previous works, were 100 twins instead.

To date, the crystallographic growth directions of the five twin laws have been described and their twinning energies determined (Rubbo et al., 2012a, 2012b). Therefore, we believe that re-investigating gypsum habit in a pure system is needed, focusing on the identification of twin laws and their habit descriptions.

Starting from a solution saturated in $CaSO_4 \cdot 2H_2O$, when evaporation occurs gypsum crystals precipitate. Gypsum precipitation by evaporation is the most common phenomenon in natural environments, and the most easily reproducible process in laboratory. Moreover, by modifying the evaporation rate (ER, hereinafter), it is possible to observe whether and how gypsum habit changes.

Here, we have replicated evaporation experiments, paying attention to the ER; i.e., a pure solution saturated in $CaSO_4 \cdot 2H_2O$ has been left to evaporate at different ERs. Acicular single crystals, curved ones, and twins showing the 100 and $\bar{1}01$ penetration twin laws have been observed. Our results, based on the precipitation frequencies, indicate that the occurrence of the 100 penetration twin law decreases with increasing ER, whereas the opposite is true for the $\bar{1}01$ penetration twin law. Furthermore, two different habits related to the $\bar{1}01$ penetration twin law have been detected: a “cruciform” habit with a visible compenetration between the parent and twinned crystals, and a “butterfly” one where the compenetration is not visible. The formation of 100 and $\bar{1}01$ penetration twin laws is also promoted by tannic acids and α-amylase enzyme, which are commonly found in sedimentary environments (Cody and Cody, 1988, 1989a); hence, both types of penetration twins may occur in evaporitic-sedimentary environments. Moreover, the crystals aspect ratio (length/width crystal ratio, AR hereinafter) could potentially serve as a quick and useful tool for distinguishing between 100 and $\bar{1}01$ penetration twins.

Previous crystal growth experiments associated the curved habit of gypsum with specific impurities dissolved in solution (Rinaudo et al., 1989; Punin and Artamonova, 2001). Moreover, our findings suggest that high ER can also promote the curvature, and a homo-epitaxial mechanism may be involved in the formation of the asymmetric curved habit.

2.2. Materials and methods

$CaSO_4 \cdot 2H_2O$ reagent plus (≥99% Sigma Aldrich), and ultrapure water (18 MΩ; obtained by using an Elga Purelab Flex3 water purification system) have been used to prepare a $CaSO_4 \cdot 2H_2O$ saturated solution at room temperature (20°C). Evaporation experiments have been performed at 20, 30 and 40°C. The related $CaSO_4 \cdot 2H_2O$ solubility values, as well as the conductivity, have been calculated using PHREEQC v3.6.3 version (Parkhurst and Appelo, 2013) and the default phreeqc database.

$CaSO_4 \cdot 2H_2O$ saturated solution has been prepared by adding 5.0 g/L of $CaSO_4 \cdot 2H_2O_{(s)}$ to water, so exceeding the gypsum saturation in pure water (2.54 g/L at 20°C). Then, $CaSO_4 \cdot 2H_2O_{(s)}$ has been kept stirring in the flask for 15 days, to ensure saturation. Solution saturation has been verified by conductivity measurements; when the conductivity value does not change significantly during time, saturation is reached. We have measured 2030 µS/cm as a stable value, slightly higher than the theoretical one (i.e., 2000 µS/cm). The solution pH was 5.4 and measured with a HANNA HI211 pH-meter. Therefore, the solution has been filtered using a cellulose filter with a pore size of 0.45 µm to remove any $CaSO_4 \cdot 2H_2O$ particles.

Four different experimental conditions have been investigated (G1-G4) and for each condition three replicas have been carried out. The maximum and minimum values of evaporation rates associated with each experimental condition are given in the main text; see appendix B (Fig. S1-S4) for the evaporation rate associated with each replica:

i) In G1, ≈30 g of solution have been stored in a 5-cm diameter beaker, covered with a perforated parafilm, and allowed to evaporate at room temperature ($0.022<ER<0.030$ g_{H2O}/hour).

ii) In G2, ≈30 g of solution have been stored in a 5-cm diameter beaker, without the parafilm cover, and allowed to evaporate at room temperature ($0.072<ER<0.082$ g_{H2O}/hour).

iii) In G3, ≈30 g of solution have been stored in a 5-cm diameter beaker, and allowed to evaporate in a ventilated oven at 30°C ($0.79<ER<1.05$ g_{H2O}/hour).

iv) In G4, ≈30 g of solution have been stored in a 5-cm diameter beaker, and allowed to evaporate in a ventilated oven at 40°C ($1.59<ER<1.94$ g_{H2O}/hour).

For each experiment, the ER has been calculated by measuring the weight of the solution at different times with an analytical laboratory balance, with a precision until the tenth of a milligram. However, we have considered only the values up to the second decimal place. Due to evaporation, the third and fourth decimal place did not provide stable values, especially in G3 and G4 solutions in which the beaker has been, each time, kept out to the oven, the weight rapidly sampled, and then re-insert into the oven to limit the cooling of the solution.

When the temperature increases, gypsum solubility slightly increases as well, and thus G3 and G4 solutions are slightly unsaturated with respect to $CaSO_4 \cdot 2H_2O$. From 20 to 30°C the solubility increases by ~0.09 g/L (2.63 g/L at 30°C), whereas at 40°C the solubility increases by 0.12 g/L (2.66 g/L at 40°C). If we consider the lowest ER among those measured in G3 and G4 experimental conditions, after 6.8 and 4.5 minutes the saturation is re-reached in G3 and G4, respectively, corresponding to a loss of 89.5 mg (G3) and 112.5 mg (G4). Hence, increasing the temperature from 20 to 30 or 40 °C does not modify the solubility of gypsum to the point of altering the outcomes of our experiments.

Solutions have been allowed to evaporate up to about one half of the sample weight. Precipitated crystals have been recovered and washed with ultrapure water, dried overnight at

room temperature, and then analyzed by optical (Olympus BX4 with JENOPTIC ProgResC5 digital camera), and electron microscopy (JEOL-JSM-IT300LV- SEM), equipped with secondary electrons and backscattered electrons (SE and BSE, respectively) detectors, and Energy-Dispersive X-Ray spectrometer (EDS).

From the evaporation of the G1-G4 solutions, both single and twinned habits of gypsum crystals have been obtained. The related twin laws have been identified by measuring the extinction angle with the optical microscope using crossed polarizers.

Fifty optical images of gypsum twins have been taken, analyzed with ImageJ image processing software, and their AR calculated (Appendix B; Fig. S5; Table S1-S2). For each experimental condition, the precipitation frequencies of the different twin laws have been measured based on eighty twins detected in each replica. The average percentage value of these measurements is reported in the main text along with the absolute error.

2.3. Results and discussions

2.3.1. Geometric-crystallographic background to identify the different gypsum twin laws and habits

Due to structural constraints, five twin laws are obtained for gypsum and the P-T individuals are mutually related by one of the following twin operations: rotation of 180°, mirror plane, or inversion center (Follner et al., 2002). Each twin law is described by a contact and penetration twin (Rubbo et al., 2012a, 2012b), thus, at least ten different twin habits are related to gypsum (Fig. 6). Geometrically, each twin law is characterized by a specific re-entrant angle (Fig. 6). By measuring its value, we can identify the twin law. However, the 100 and $\overline{1}01$ twin laws have the same re-entrant angle (i.e., 105.02°). Thus, goniometry cannot distinguish these twins and the formal way to correctly identify the 100 and $\overline{1}01$ twin laws require the measurement of the extinction angle (Δ) formed between the two individuals, by means of optical microscopy in crossed polarizers. This angle is 14° and 26° for 100 and $\overline{1}01$ twin laws, respectively. Finally,

a re-entrant angle and an arrowhead at opposite sides indicate a contact twin (Rubbo et al., 2012a), while two re-entrant angles observed at the opposite twin sides, identify a penetration twin (Rubbo et al., 2012b).

TWIN LAWS	CONTACT TWINS	Character of the OCP (contact)	PENETRATION TWINS	Character of the OCP (penetration)	θ	Δ
100	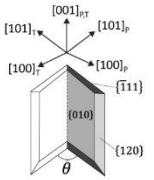	100 - S	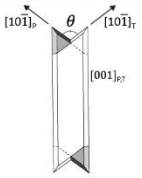	010 - F	105°	14°
$\bar{1}01$	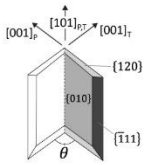	$\bar{1}01$ - S	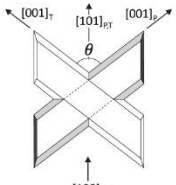	010 - F	105°	26°
001	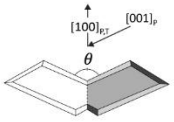	001 - S	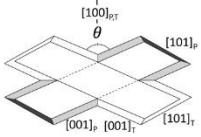	010 - F	132°	27°
$20\bar{1}$	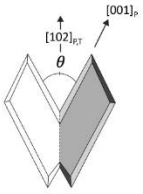	$20\bar{1}$ - K	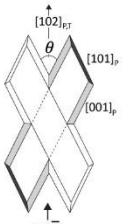	010 - F	53°	24°
101	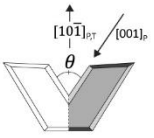	101 - K	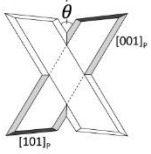	010 - F	62°	43°

Figure 6 Geometry of contact and penetration twins, viewed along the [010] direction of gypsum. Modified from Rubbo et al. (2012a, b). Twin laws: 100, $\bar{1}01$, 001, $20\bar{1}$, and 101. The "character of the OCP" (i.e., the character of the Original Composition Plane) refers to the crystallographic form {*hkl*} where the nucleation of a twinned growth unit occurred. For each twin law, the re-entrant angle value (θ) and the optical extinction angle value (Δ) have been reported. The extinction angles (Δ) were measured having adopted the structure defined by de Jong and Bouman (1939). The steps followed to measure the extinction angles are reported in the Appendix B, Fig. S6-S7. Subscripts "P" and "T" identify the two individuals, Parent and Twinned, making the twin.

2.3.2. The effect of different evaporation rates on gypsum habit

At slowest evaporation rate (G1 solution: 0.022<ER<0.030 g_{H2O}/hour), single crystals [001] elongated, 100 and $\bar{1}01$ penetration twins have been detected (Fig. 7A-C). The precipitation frequencies of 100 and $\bar{1}01$ gypsum twin laws are as follows: 45.4±1.8% for the 100 penetration twin law and 54.6±1.8% for the $\bar{1}01$ penetration one. When increasing the ER (G2 solution: 0.072<ER<0.082 g_{H2O}/hour), we have obtained the precipitation of acicular crystals, and twinned crystals showing the 100 and $\bar{1}01$ penetration twin laws (Fig. 7A-D). $\bar{1}01$ penetration twin law shows two different habits: the "cruciform" habit with a visible compenetration between the two individuals forming the twin, already detected in G1 solution (Fig. 7C), and a "butterfly" one with a not visible compenetration (Fig. 7D). In addition, the precipitation frequencies of the twin laws slightly changed with respect to the G1 solution: 19.6±3.8% for the 100 penetration twin law, 75.8±3.8% for the $\bar{1}01$ penetration twin law with a cruciform habit, and 4.6±1.3% for the $\bar{1}01$ penetration "butterfly" twin law. At higher evaporation rates (ER≥0.79 g_{H2O}/hour) we have obtained the precipitation of acicular crystals, $\bar{1}01$ penetration twin law with butterfly habit, and curved crystals (Fig. 7A, D-F). 100 and $\bar{1}01$ penetration twin law with cruciform habit have not been detected. Curved crystals exhibit both "symmetric" (Fig. 7E) and "asymmetric" curvature (Fig. 7F). The symmetrically curved habit is characterized by two main curvatures, at opposite crystal sides, symmetrically related by means of a rotation of 180° or an inversion center, whereas the asymmetrically curved habit is characterized by only one main curvature. The occurrence of different gypsum crystal habits, and precipitation frequencies of twin laws as function of ERs are sketched in Fig. 8.

Based on these findings, the precipitation frequencies of both 100 and $\bar{1}01$ penetration twins depend on the ER, and the $\bar{1}01$ penetration twin law can precipitate with two different habits (Fig. 7C, D), whose precipitation frequency is related to the ER as well. Using the rich statistical

data on the penetration growth twins described in literature, Rubbo et al. (2012b) calculated the different habits of penetration twins. They observed that the 100 penetration twins are more elongated when compared to $\overline{1}01$ ones, and thus the AR should be a fast and useful parameter to distinguish these twin laws. To test this hypothesis, we have measured the AR of fifty 100 and $\overline{1}01$ penetration twins (Appendix B, Fig. S5; Table S1). Based on this dataset, only 100 penetration twins have showed an AR>2.51±0.02, whereas exclusively $\overline{1}01$ penetration twins show an AR<1.97±0.01 (Appendix B, Table S2; Fig. 9). In the range 1.97<AR<2.51, aspect ratio of both 100 and $\overline{1}01$ penetration twin laws are measured and thus this range does not allow to distinguish between the two. Therefore, the AR parameter might be a fast and useful tool to distinguish between 100 and $\overline{1}01$ penetration twins.

The curved habit of gypsum, also known as “bent habit”, has already been reported in the literature. To our knowledge, two different experimental growth conditions can promote the curvature in gypsum crystals: diffusion-controlled experiments in the presence of impurities, and evaporation experiments in the presence of impurities (Rinaudo et al., 1989; Punin and Artamonova, 2001). The proposed formation mechanism suggests that impurity absorption triggers structural defect and crack formation in gypsum during crystal growth (Rinaudo et al., 1989; Punin and Artamonova, 2001). It has been proposed that cracks and defects promote the nucleation and growth of a new gypsum crystallite with a different crystallographic orientation with respect to the former crystal; as a result, the overall habit of the aggregated crystals at the growth front is bent, as shown in Fig. 7E, F. Our experiments reveal another growth attribution to curved crystals, which occurs when a solution rich in Ca^{2+} and SO_4^{2-} ions rapidly evaporate without any impurities dissolved. In this case, crack formation may be promoted by high ER. Importantly, our set of experiments has been conducted at different temperatures, hence the bending could be related to an increase in evaporation rate, temperature, or a combination of both. Oddly, the specific effect of temperature on gypsum habit has not been investigated yet.

Specific and quantitative analyses should be carried out to provide reliable information on the temperature-gypsum habit relationship. Against the involvement of temperature in promoting the curvature, we point out that in diffusion controlled growth experiments, curved crystals have been obtained at room temperature (Punin and Artamonova, 2001), and Rinaudo et al. (1989) observed the curvature at 25, 35, and 45°C. Moreover, different growth experiments dealt with gypsum precipitation at temperatures ranging between 5-60°C (although many other variables were involved), but curved crystals have never been described (Cody, 1976; Cody and Cody, 1988). Therefore, we can provisionally assume that temperature is not involved in promoting the curvature, but rigorous analyses are needed.

Finally, it is pivotal to note that the curved habit of gypsum is not only an artefact of crystal growth of laboratory experiments but is observed in natural environments too (Wenrich and Sutphin, 1994; Panczner, 1987; Bąbel et al., 2015). Based on the findings described here, we suggest considering the evaporation rate as a plausible parameter in promoting the curved habit in natural environments and overall, in evaporitic settings.

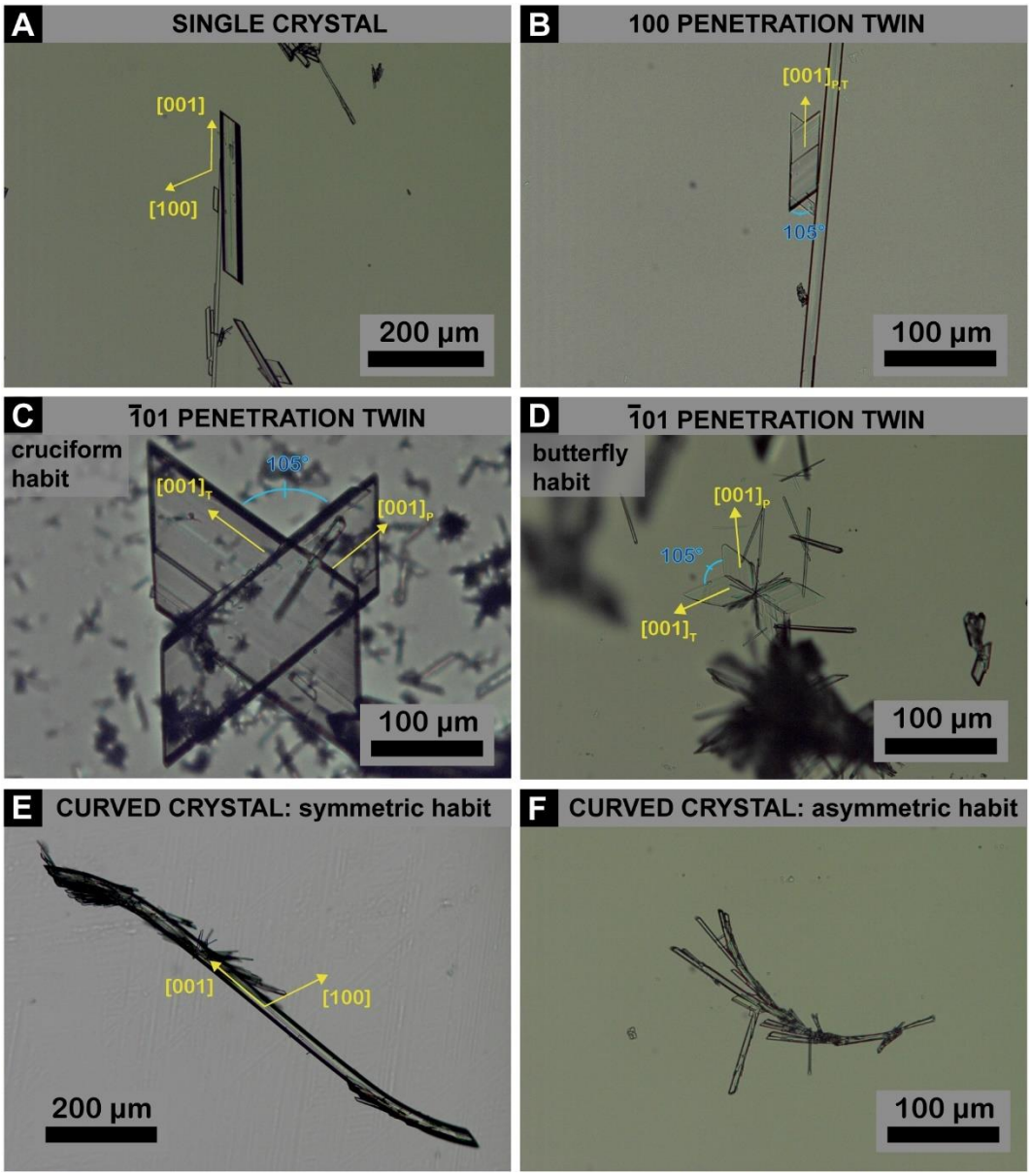

Figure 7 Gypsum habits detected in G1-G4 experiments. A re-entrant angle of 105° identifies both 100 and $\bar{1}01$ twin laws; two re-entrant angles at opposite sides identify a penetration twin. By measuring the different extinction angles of the reported 100 and $\bar{1}01$ penetration twins (i.e., 14° and 26° for 100 and $\bar{1}01$ twin law, respectively) we can distinguish the two twin laws. Subscripts "P" and "T" identify the two individuals, Parent and Twinned, composing the twin. A) Acicular single crystal. B) 100 penetration twin. C) $\bar{1}01$ penetration twin with a cruciform habit. D) $\bar{1}01$ penetration twin with a butterfly habit. E) Symmetrically curved crystal. F) Asymmetrically curved crystal.

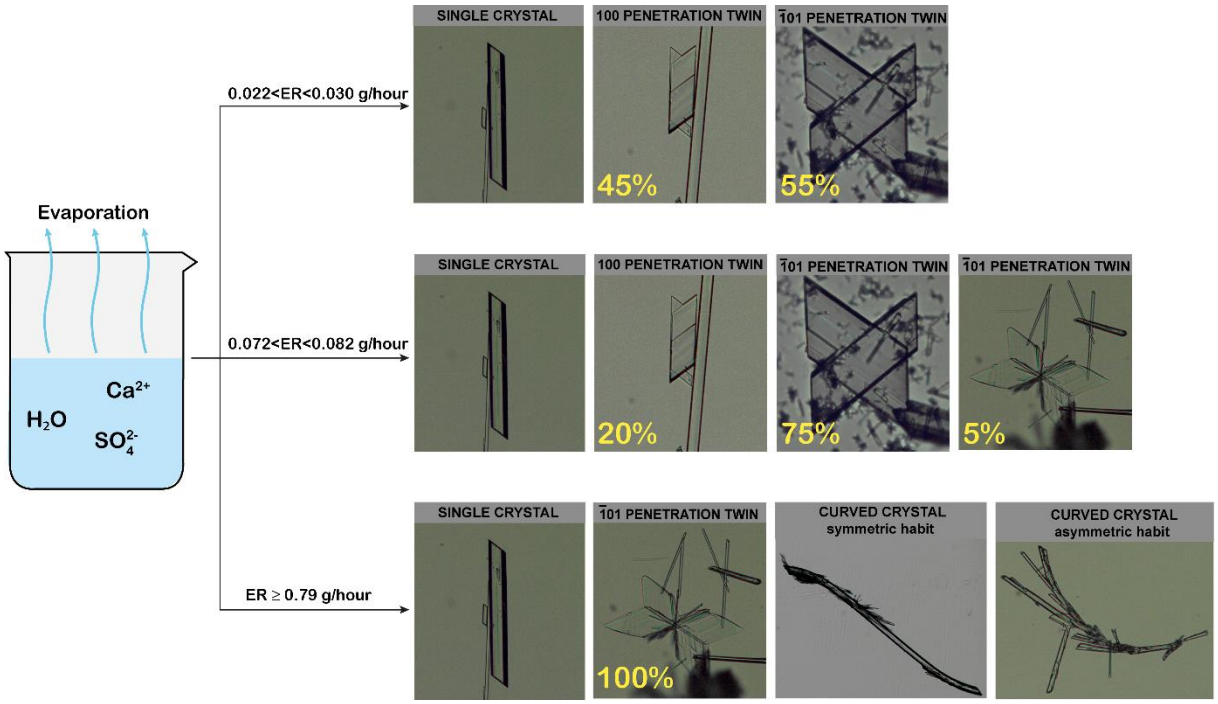

Figure 8 Gypsum crystal habits and twin laws precipitation frequencies as a function of ERs. For the sake of simplicity, the percentage values shown in the figure have been approximated to unity. Refer to the main text for values approximated to the first decimal place.

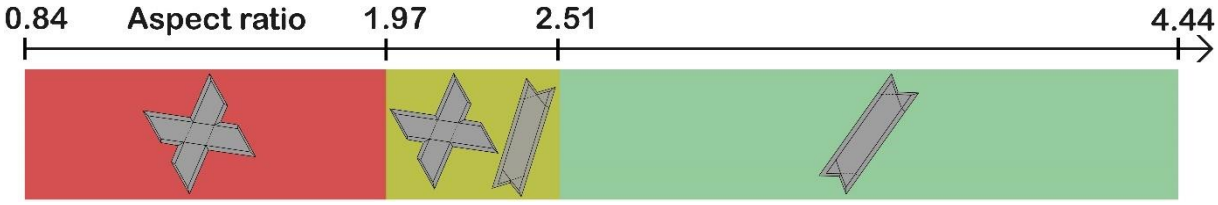

Figure 9 Distribution of the 100 and $\bar{1}01$ penetration twin laws as function of the aspect ratio.

2.3.3. Hypothetical morphogenetic mechanism of the asymmetric curvature

Intriguingly, in the symmetrically "curved" habit the two curvatures are symmetrically related by means of a rotation of 180° or an inversion center. Hence, Rinaudo et al. (1989) have suggested a twin mechanism, promoted by cracks formation, to explain the observed habit. However, only crystallographic consideration has been carried out, and thus further computational and experimental analyses should be performed to strengthen this growth model.

In contrast, the asymmetrically curved habit shown in Fig. 7F cannot be explained by a twin mechanism because there is not a twin operation related to the growth shape (Klein et al., 1993; Nesse, 2012). This habit arises from the overlapping of crystals with different orientations (from 8° to 25°) between the direction of one crystal and its neighboring (Fig. 10). To explain this crystal curvature, a homo-epitaxial mechanism may be involved, where systematic rotations of the common 2D coincidence cells occur. This growth mechanism does not require a twin operation. Indeed, in a homo-epitaxial mechanism two or more crystallographic forms {hkl} and {h'k'l'}, of the same crystal species, can associate in an epitaxial relation without producing a new twin law (Bruno et al., 2022a). Referred to curved crystals, the crystallographic forms involved in the homo-epitaxy could be the {010}, {120}, or generally, the {1k0} (Massaro et al., 2011), considering crystals are compenetrated one each other, therefore crystallographic forms (not detectable by imaging) could be involved (Fig. 11). We have investigated the 2D coincidence cells occurring between two 010 planes, by rotating one plane up from 8° to 25°. Geometrically, we have found that there are many different positions coherent with the constraints required for epitaxy interaction (i.e., linear and area misfit < 14%) (Table 1) (Mutaftschiev, 2001). The multitude of 2D coincidence cells satisfying epitaxial constraints agrees with the angular misfit variety measured on our curved crystals, therefore, a homo-epitaxial mechanism may be involved in the formation of the asymmetric curved habit.

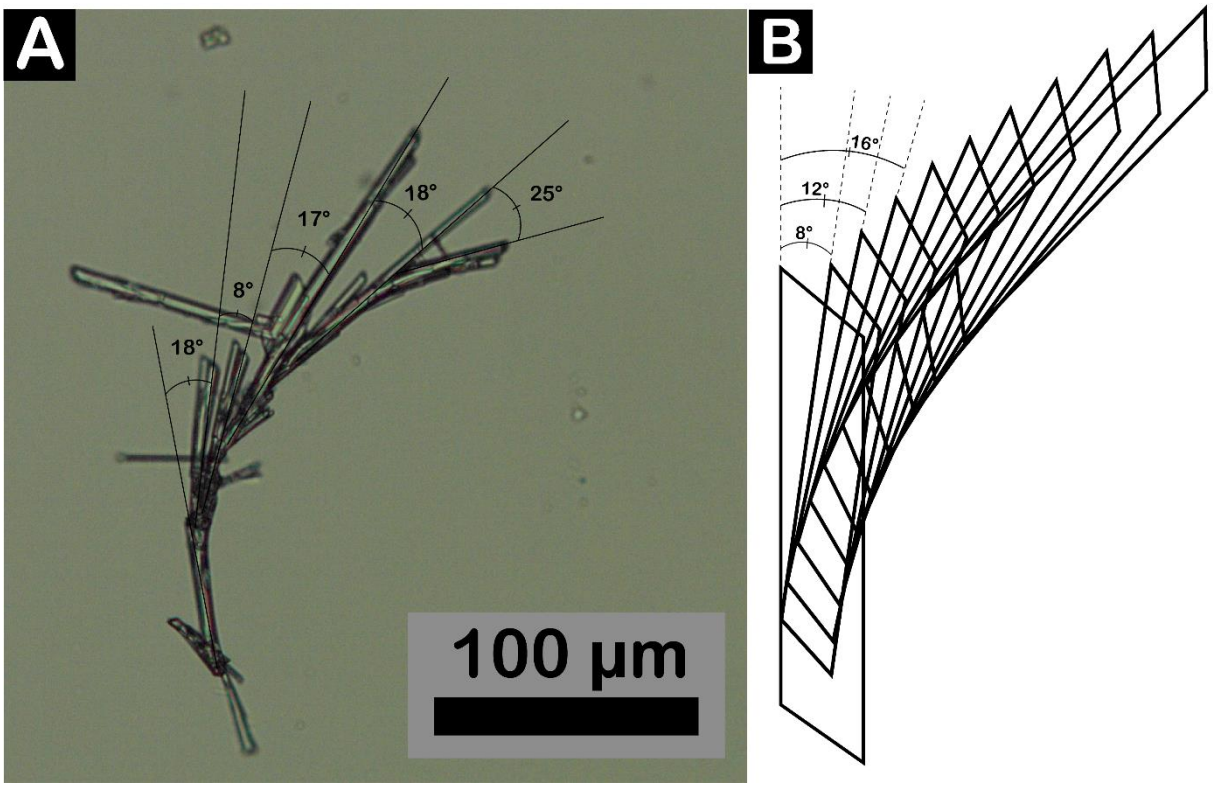

Figure 10 A) The angular misfit between the direction of one crystal and its next/previous one composing the asymmetric curved habit range between 8° and 25°. The reported angular values should be considered within a confidence interval of about ±2°. B) Sketch of the curvature. A small angular misfit between the direction of one crystal and its neighboring produces the curved habit.

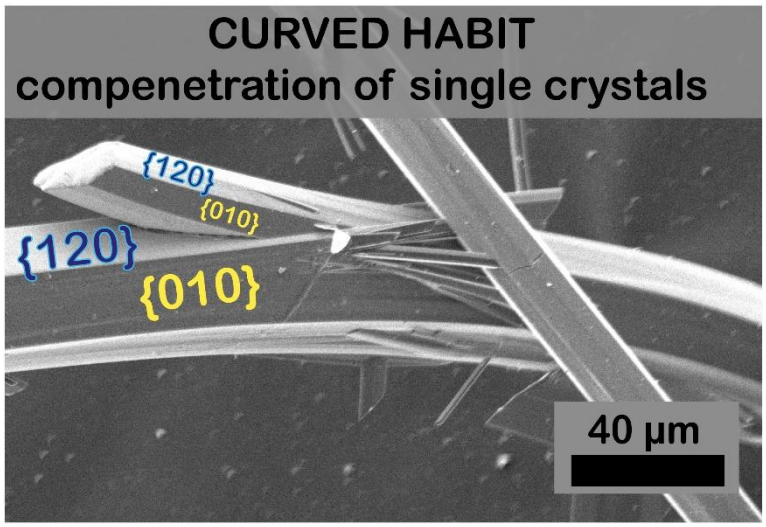

Figure 11 The crystals composing the curved habit cross one another sharing the {010} and the {120} crystallographic forms.

Table 1. 2D coincidence cells of two 010 planes when one plane rotates from 8° to 25°.[a]

Rotation angle (°)	Directions	Linear misfit (%)	Area misfit (%)
8°	[307]≡[207]	-1.2%	3.5%
	[702]≡[703]	+0.8%	
9°	[306]≡[206]	-0.4%	<1.0%
	[702]≡[703]	+0.8%	
10°	[306]≡[206]	-0.4%	<1.0%
	[702]≡[703]	+0.8%	
11°	[305]≡[205]	+1.0%	≈0%
	[702]≡[703]	+0.8%	
12°	[305]≡[205]	+1.0%	≈0%
	[602]≡[603]	-1.3%	
13°	[204]≡[104]	-1.4%	≈16.5%
	[501]≡[502]	-15.2%	
14°	[204]≡[104]	-1.4%	≈16.5%
	[501]≡[502]	-15.2%	
15°	[204]≡[104]	-1.4%	≈0%
	[401]≡[402]	-0.5%	
16°	[204]≡[104]	-1.4%	≈0%
	[401]≡[402]	-0.5%	
17°	[203]≡[103]	+2.0%	<1.0%
	[401]≡[402]	-0.5%	
18°	[203]≡[103]	+2.0%	<1.0%
	[401]≡[402]	-0.5%	
19°	[203]≡[103]	+2.0%	<1.0%
	[401]≡[402]	-0.5%	
20°	[203]≡[103]	+2.0%	<1.0%
	[401]≡[402]	-0.5%	

21°	[203]≡[103]	+2.0%	<1.0%
	[401]≡[402]	-0.5%	
22°	[305]≡[105]	-1.5%	≈0%
	[601]≡[603]	+1.2%	
23°	[102]≡[002]	-9.5%	≈2.0%
	$[\bar{1}02]\equiv[\bar{2}01]$	+4.2%	
24°	[102]≡[002]	-9.5%	≈1.0%
	$[\bar{1}02]\equiv[\bar{2}01]$	+4.2%	
25°	[102]≡[002]	-9.5%	≈8.5%
	$[\bar{5}03]\equiv[\bar{7}00]$	+0.2%	

[a] Only for a rotation of 13° and 14° the constraints required for epitaxy (i.e., linear and area misfit < 14%) are not satisfied.

2.3.4. Mineralogical implication: do the "swallowtail" gypsum twins represent different twin laws?

Gypsum precipitation through evaporation was a common process in ancient sedimentary basins involved in the evaporitic events that occurred on Earth history (Warren, 2010). Notwithstanding, 100 and $\bar{1}01$ penetration twins have never been identified in the sedimentary successions deposited in response to these dramatic modifications of basinal hydrologic balance. These complex chemical environments – rich in organic and inorganic compounds deriving, for instance, from both planktonic and benthonic biological activity (Dela Pierre et al., 2015; Pellegrino et al., 2021; Natalicchio et al., 2022) – may have selected different twin laws of gypsum with respect to the 100 and $\bar{1}01$ penetration ones. However, crystal growth experiments claim that specific organic molecules commonly found in sedimentary environments (tannic acid, deriving from the decomposition of leaves; α-amylase, an enzyme excreted into soils and water by bacteria, fungi, algae, plant roots) promote the formation of 100 and $\bar{1}01$ penetration twin laws (Cody and Cody, 1988, 1989a). Therefore, there is

apparently no valid reason why 100 and $\overline{1}01$ penetration twins cannot be observed in modern and ancient sedimentary successions. We propose that 100 and $\overline{1}01$ penetration twins have been observed in nature but inappropriately defined as "swallowtail twins", which is the terminology commonly used to identify gypsum twinned crystals with a shape at a first glance similar. Therefore, we strongly suggest improving the identification of the different gypsum twin laws observed in nature, as they may serve as proxy for the chemistry of the original water from which gypsum precipitated, hence, contributing to the interpretation of the gypsum depositional environment in ancient deposits.

2.3.5 The curved gypsum habit: from laboratory experiments to natural environment

The naturally occurring curved gypsum crystals are commonly called ram's horn gypsum, described in cave environments (Fig. 5D; Wenrich and Sutphin, 1994; Panczner, 1987) and sabre gypsum observed in ancient gypsum deposits (e.g., Badenian gypsum of eastern Europe; Fig. 5E; Bąbel et al., 2015)

Ram's horn gypsum habit is described as an aggregate of parallel acicular crystals that lie in the curving plane showing different orientations (Wenrich and Sutphin, 1994; Panczner, 1987). This description agrees with the curved habit obtained in our experiments. This morphological affinity makes the exploration of the ram's gypsum formation particularly interesting. Redox reactions related to the sulfur cycle can occur in caves: the oxidation of hydrogen sulfide (H_2S) to sulfuric acid (H_2SO_4) and subsequent limestone dissolution is responsible for the sulfuric acid speleogenesis (SAS) and sulfur speleothems formation. This process produces $Ca^{2+} - SO_4^{2-}$ rich waters undersaturated with respect to gypsum (Engel et al., 2004). Consequently, subsequent evaporation of $Ca^{2+} - SO_4^{2-}$ rich waters produced by SAS in caves may generate the ram's horn gypsum habit. The appropriate evaporation rate required to

trigger ram's horn gypsum precipitation might be generated by the constant air flows often characterizing cave environments (Badino and Chignola, 2019; Gomell and Pflitsch, 2022).

Sabre gypsum crystals have been described in Badenian (Miocene) evaporitic deposits of Eastern Europe (Bąbel et al., 2015). The unidirectional curvature of the crystals was interpreted as a consequence of flowing brines, causing the preferential growth of crystal faces upstream (Bąbel and Becker, 2006). However, other factors can promote the curved crystal habits. As already hypothesized for ram's horn gypsum, a transient increase in the evaporation rate of $Ca^{2+} - SO_4^{2-}$ rich waters - ubiquitous phenomenon in evaporitic environments - may be involved in the formation of curved habit.

2.4 Conclusions

The effect of evaporation rate on gypsum habit has been investigated by carrying out four batches of experiments at four different evaporation rates: different gypsum habits as a function of evaporation rates have been detected.

By increasing the evaporation rate, the formation of the $\overline{1}01$ penetration twin law is favored with respect to the 100 penetration one, and the $\overline{1}01$ penetration twin law can occur with two different habits whose precipitation frequencies are related to the evaporation rate as well. Previous experiments disclosed the formation of 100 and $\overline{1}01$ twinned gypsum crystals in the presence of organic molecules characteristics of sedimentary environments (Cody and Cody, 1988, 1989b). Consequently, these twin laws can be detected in evaporitic-sedimentary environments. Aimed at favoring researchers to identify the twin laws of gypsum crystals, we have proposed the measurement of crystal aspect ratio (length/width crystal ratio) as a potential fast and useful tool to distinguish between 100 and $\overline{1}01$ penetration twins.

At higher evaporation rates (ER≥0.79 g_{H2O}/hour) curved crystals exhibit both "symmetric" and "asymmetric" curvatures. Based on crystallographic considerations, Rinaudo et al. (1989) suggested a twin mechanism may promote the symmetric curvature, whereas we have

hypothesized a homo-epitaxial mechanism for the asymmetric one. Moreover, until today, the crystal curvature has been related with impurities absorption (Rinaudo et al., 1989; Punin and Artamonova, 2001), but another growth attribution has been here documented, independent from the chemical environment and only related to supersaturation. Based on these findings, we raised the question whether the curved gypsum habits observed in natural environments may be generated by the rapid evaporation of $Ca^{2+} - SO_4^{2-}$ rich waters.

To summarize, these experimental findings provide the first evidence of different gypsum habits as a function of evaporation rates in a pure system. Acicular single crystals, curved crystals, 100 and $\overline{1}01$ penetration twins are the habits detected. When the effect of additives on gypsum habits is explored by performing crystal growth experiments, and when different gypsum habits are analyzed in evaporitic environments, this wide array of habits should be considered.

Chapter 3

$\bar{1}01$ contact twins in gypsum experimentally obtained from calcium carbonate enriched solutions: mineralogical implications for natural gypsum deposits

3.1. Introduction

Gypsum twins are frequently observed in nature triggered by a wide array of impurities which are present in their depositional environments and may exert a critical role in the selection of different twin laws. Identifying the impurities able to promote the selection of specific twin laws has relevant implications for the geological studies aimed at interpreting the gypsum depositional environments in ancient and modern deposits.

Recently, an epitaxial relationship between the {010} pinacoid of gypsum and the {10.4} rhombohedron of calcite (Ruiz-Agudo et al., 2016; Aquilano et al., 2022) has been demonstrated. Therefore, the effect of carbonate anions – ubiquitous in evaporitic environments - on the habit of gypsum crystals deserves further investigation. Consequently, the main goal of this part of the work is to explore the effect of calcium carbonate (Ca-carbonate, hereinafter) on gypsum habit by performing temperature-controlled laboratory experiments from aqueous solutions in the presence of calcium carbonate, comparing it with the pure calcium sulfate system. Our results indicate that an aqueous solution saturated in Ca-carbonate promotes the precipitation of twinned gypsum following the $\bar{1}01$ contact twin law. This is the first evidence of the effect of Ca-carbonate as a specific impurity promoting the formation of the $\bar{1}01$ contact twin law. To support the formation of this twin law, we must stress that a mixed phase carbonate/sulfate called rapidcreekite was detected as a precursor in gypsum precipitation when carbonate species are dissolved in solution (Bots, 2011). The structural affinities between gypsum and rapidcreekite suggest that this latter could act as a precursor of gypsum via an epitaxial mechanism, promoting the formation of the $\bar{1}01$ gypsum contact twin law.

Finally, we propose that the orientations of the negative crystal-shape of primary fluid inclusions (FIs) with respect to the twin plane and the main elongation of the sub-crystals making the twin, are a useful tool to distinguish between 100 and $\overline{1}01$ twins, which can be relevant for the interpretation of ancient gypsum deposits.

3.2. Materials and methods

$CaSO_4 \cdot 2H_2O$ reagent plus (≥99% Sigma Aldrich), $CaCO_3$ ACS reagent (≥ 99% powder, Sigma-Aldrich), and ultrapure water (18 MΩ; obtained by using an Elga Purelab Flex3 water purification system) were used to prepare i) a $CaSO_4 \cdot 2H_2O$ saturated solution (G1) and ii) a $CaSO_4 \cdot 2H_2O - CaCO_3$ saturated solution (G2). Both G1 and G2 were saturated at 40°C. A cryo-compact Julabo circulator (CF31 series) was used to keep the solution at 40°C. Solubility values of $CaSO_4 \cdot 2H_2O$ at 40°C and 4°C were calculated using PHREEQC v3.7.3 version and the default phreeqc database.

G1 was prepared by adding solid $CaSO_4 \cdot 2H_2O$ in amounts exceeding the saturation in pure water at 40°C (i.e., 2,66 g/L). G2 was prepared by adding $CaSO_4 \cdot 2H_2O$ in amounts exceeding its saturation in pure water at 40°C, to a solution already saturated with Ca-carbonate. Under these conditions, the surplus of $CaCO_3$ and $CaSO_4 \cdot 2H_2O$ was kept stirring in the flask for 15 days to ensure that saturation had been reached.

The pHs of G1 and G2 were 5.6 and 7.8, respectively. The pH of G2 is higher with respect to that of G1 due to the basic hydrolysis of carbonate ions. pH measurements were carried-out with a HANNA HI211 pH-meter.

Before the crystallization experiments, G1 and G2 were vacuum filtered in a beaker pre-heated to 40°C, to avoid rapid crystal precipitation, using a cellulose filter with a pore size of 0.45 μm to remove larger pre-existent $CaCO_3$ and $CaSO_4 \cdot 2H_2O$ particles.

100 mL of G1 and G2 were put in a refrigerator set at 4°C for 30 days, in closed flasks to avoid evaporation. The gypsum precipitation was achieved through different $CaSO_4 \cdot 2H_2O -$

$CaCO_3$ solubilities as a function of temperature. Indeed, lowering the temperature from 40 to 4°C determines a decrease in gypsum solubility – from 2.66 g/L to 2.29 g/L – and an increase in $CaCO_3$ solubility (Plummer and Busenberg, 1982; Coto et al., 2012). Thus, Ca-carbonate minerals do not precipitate whereas both nucleation and growth of gypsum crystals occur.

Crystals were washed with ultrapure water, dried overnight at room temperature, and then analyzed by optical (Olympus BX4 with JENOPTIC ProgResC5 digital camera), and electron microscopy JEOL-JSM-IT300LV- SEM, equipped with a secondary (SE), backscattered electron (BSE), and an Energy-Dispersive X-Ray spectrometer (EDS).

3.3. Results and Discussions

3.3.1. Gypsum twin growth morphologies

From the G1 solution (saturated in $CaSO_4 \cdot 2H_2O$) we obtained the precipitation of i) acicular single crystals [001] elongated (Fig. 12A); ii) 100 penetration twins with the two re-entrant angles developing along [001] and $[00\bar{1}]$ (Fig. 12B); and iii) $\bar{1}01$ penetration twins with the two re-entrant angles developing along [101] and $[\bar{1}0\bar{1}]$ (Fig. 12C).

From G2 solution (saturated both in $CaSO_4 \cdot 2H_2O$ and $CaCO_3$) we obtained the precipitation of acicular crystals, 100 penetration twins and $\bar{1}01$ penetration twins (described above in G1 solution), and a new twin morphology. Fig. 13A shows a twin characterized by a re-entrant angle of 105°, and an optical extinction angle of 26° measured by means of optical microscopy (see Appendix C, Fig.S1, for the optical microscopy image). Moreover, a re-entrant angle at one side and an arrowhead at the opposite twin side are clearly identified. These features identify the $\bar{1}01$ contact twin law.

Both 100 and $\bar{1}01$ twin laws show the same value of the re-entrant angle. However, the sub-crystals composing 100 contact twins grow parallel to the twin plane (Otálora and García-Ruiz, 2014), whereas in $\bar{1}01$ contact twins the main elongation of sub-crystals is oriented obliquely

with respect to the twin plane (Fig. 13). Therefore, we propose that the main elongation of the sub-crystals (making the twin) with respect to the twin plane is a useful tool to distinguish between 100 and $\bar{1}01$ contact twins, especially on natural samples whose optical extinction angle is often difficult to measure.

Moreover, the multiplicity of the gypsum twin operations is 2 (rotation of 180°, mirror plane or inversion center) and thus each twin law is composed of only two sub-crystals. In contrast, the experimentally obtained $\bar{1}01$ contact twins show many sub-crystals making the twin (Fig. 13A). To explain this intriguing habit, a plausible mechanism might be the following: when the first $\bar{1}01$ contact twin is formed - composed only by two sub-crystals - its re-entrant angle is the most reactive site during growth, and thus a new $\bar{1}01$ contact twin can statistically nucleate and grow in this position. This mechanism repeated several times generates a multi-laminated twin as shown in Fig. 13.

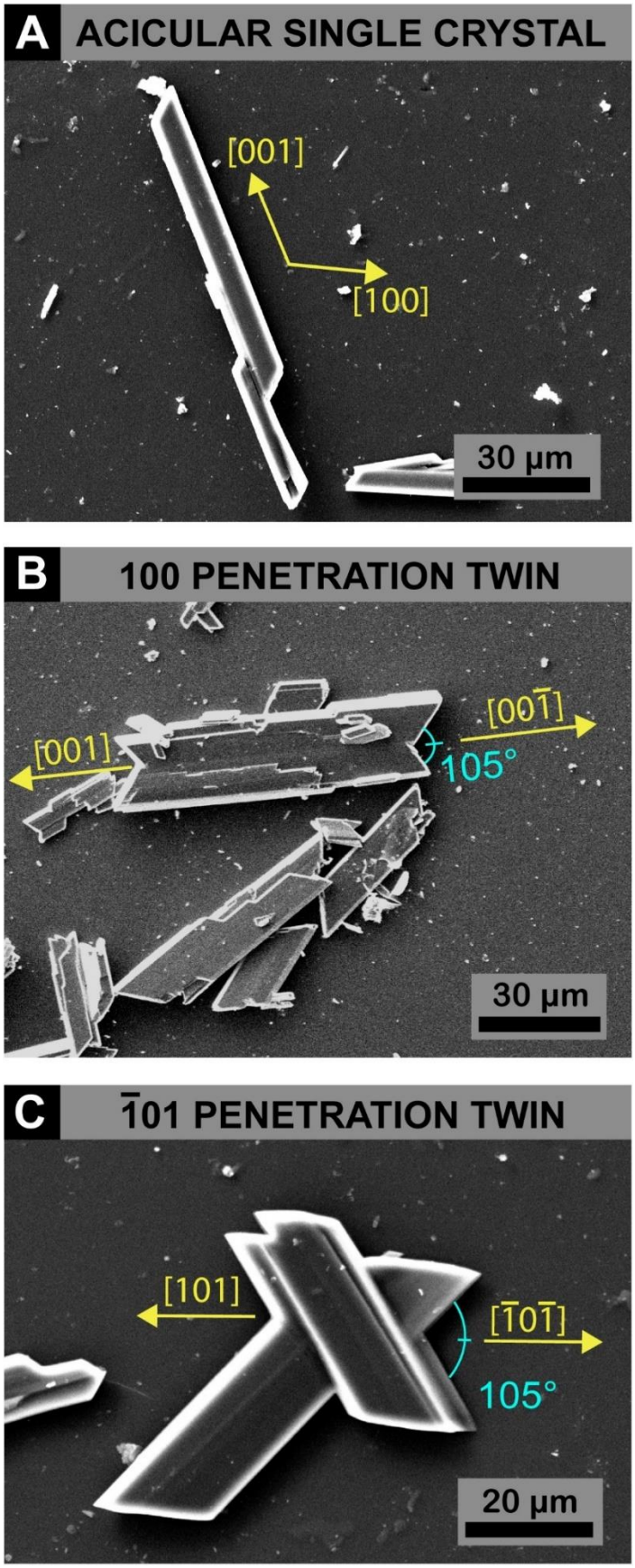

Figure 12 Gypsum crystals precipitated from G1 solution. A) Acicular gypsum single crystals. B) 100 penetration twin. C) $\bar{1}$01 penetration twin.

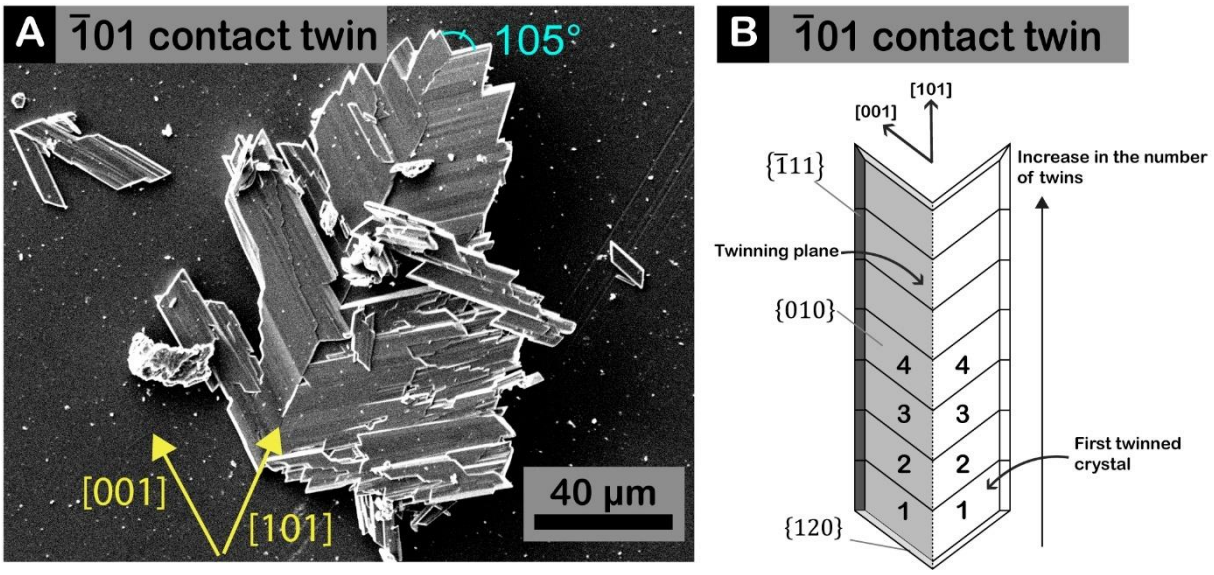

Figure 13 A) $\bar{1}$01 gypsum contact twin precipitated from a solution saturated in Ca-carbonate and calcium sulfate dihydrate (G2 solution). B) Schematic representation of the $\bar{1}$01 gypsum contact twins obtained in G2 solution.

3.3.2. The role of CO_3^{2-} ions in the formation of $\bar{1}$01 gypsum contact twin law

Rapidcreekite is a rare hydrated Ca-sulfate−Ca-carbonate compound ($Ca_2SO_4CO_3 \cdot 4H_2O$) found in association with gypsum and other carbonate minerals (Bots, 2011; Avdontceva et al., 2021). It is composed of layers of Ca – SO_4 – Ca – CO_3 with each Ca-site coordinated by CO_3, SO_4 and two H_2O groups (Cooper and Hawthorne, 1996). It belongs to the orthorhombic *Pbcn* space group and its unit-cell parameters are a_0=15.49; b_0=19.18 and c_0=6.15 Å; α=β=γ=90° (Roberts et al., 1986; Cooper and Hawthorne, 1996; Avdontceva et al., 2021).

Due to the chemical and structural affinities between gypsum and rapidcreekite structures, Cooper and Hawthorne (1996) suggested a new formation mechanism for gypsum twins. They realized that the replacement of half the sulfate groups in gypsum produces the formula of the rapidcreekite.

The resulting structure contains alternating sulfate and carbonate layers, and the sulfate groups in the alternate layers are rotated by 180º with respect to the previous one (Fig. 14).

Interestingly, the 180° rotation occurs along the [101] direction in our gypsum indexing, matching with the growth direction of the re-entrant angle in $\overline{1}01$ gypsum twins.

Moreover, gypsum crystallization affected by carbonate species in solutions was studied by Bots (2011) through *in situ* time resolved crystallization experiments using wide angle synchrotron X-ray scattering (WAXS) (I22 beamline (SAXS/WAXS) at Diamond Light Source). He observed that rapidcreekite is an intermediate product in gypsum formation.

These results agree with our experimental observations about the precipitation of $\overline{1}01$ contact twins in carbonate-rich environments.

We investigated the 2D lattice coincidences between the {100} form of rapidcreekite and the {010} form of gypsum (Table 2). Both calculated linear and area misfits satisfy the constraints required for epitaxy interaction (i.e., linear and area misfit < 14%) (Mutaftschiev, 2001), allowing to the consider of rapidcreekite as a precursor in gypsum precipitation via an epitaxial mechanism, promoting the formation of the $\overline{1}01$ contact twin law. Indeed, epitaxial growth is an acknowledged phenomenon responsible for triggering different growth morphologies (Kellermeier et al., 2012; Bruno et al., 2022a), and polymorphs even if metastable phases are involved (Bruno et al., 2022b). The host phase forms a nanometre-thick intermediate structure whose faces act as the epitaxy substrate of the stable crystal, as reported in previous research where epitaxial relationships between two phases were investigated (Bruno et al., 2022a, 2022b).

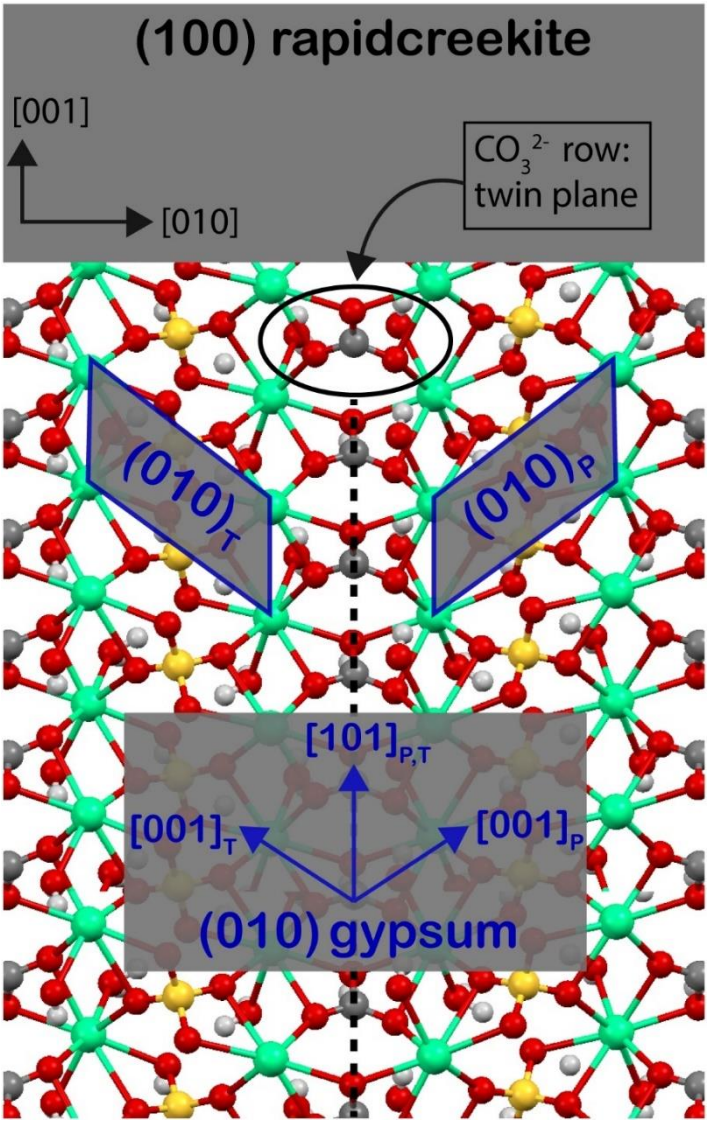

Figure 14 Projected structure of rapidcreekite perpendicular to (100) plane. It provides evidence that twinning in gypsum structure can be due to the presence of rows of carbonate groups (black dotted line). Atoms are identified with the following colors. Green: calcium; yellow: sulfur; red: oxygen; grey: carbon; white: hydrogen.

Table 2 2D lattice-coincidences between the {100} form of rapidcreekite and the monoclinic {010} gypsum form.

Rapidcreekite (100)	Gypsum (010)	Geometric misfit (%)
$[0\bar{1}2]$ = 22.78 Å	4 x [100] = 22.52 Å	-1.14%
[001] = 6.15 Å	[101] = 6.52 Å	+5.67%
2D Area = 118.23 Å^2	2D Area = 128.59 Å^2	+8.0%

3.3.3. Mineralogical implications

Marine and lacustrine waters from which gypsum precipitates are rich in carbonate in its different species. Therefore, it is relevant to explore if the $\bar{1}01$ gypsum contact twins have been observed in these evaporitic environments. Gypsum crystals occur in evaporitic environments with three different contact twin habits:

i) Prismatic habit (Fig. 15A) (Reid et al., 2021) with a re-entrant angle value ranging between 100-105° and sub-crystals parallel to the twin plane. These features identify the 100 twin law.

ii) Tabular habit (Fig. 15B), (Costanzo et al., 2019; Natalicchio et al., 2021), with a re-entrant angle value ranging between 100-105° and sub-crystals parallel to the twin plane (Bigi et al., 2022). Thus, the crystal follows the 100 twin law as shown in Fig 15A, but it is characterized by a different habit.

iii) Multi-laminated habit (Fig. 15C), commonly called "Christmas tree" (Rodríguez-Aranda et al., 1995). In Fig. 15C the re-entrant angle value range is 98-101°, closer to the re-entrant angle value of 105° related to the 100 and the $\bar{1}01$ gypsum twin laws.

Five twin laws are allowed for the gypsum structure (Follner et al., 2002), consequently only five re-entrant angle values are possible. However, it is reasonable to assume that in the natural environment gypsum crystals may be subjected to physical processes that may result in a deviation from the theoretical value of the twin law re-entrant angle, as demonstrated by natural gypsum twins shown in Figure 15.

Interestingly, in Fig. 15C the habit is composed by many specular and bladed individuals obliquely elongated with respect to the twin plane like the $\bar{1}01$ contact twins detected in G2 solution. The [001] direction (c-axis) is parallel to the elongation of the sub-crystals composing the twin; the same crystallographic directions describing $\bar{1}01$ contact twins detected in G2 are obtained. Therefore, we propose that the $\bar{1}01$ gypsum contact twins, observed in the

crystallization experiments from solutions saturated in Ca-carbonate, are present in geological evaporitic environments. The high carbonate content in brine from which evaporites precipitated could have promoted the formation of this gypsum habit.

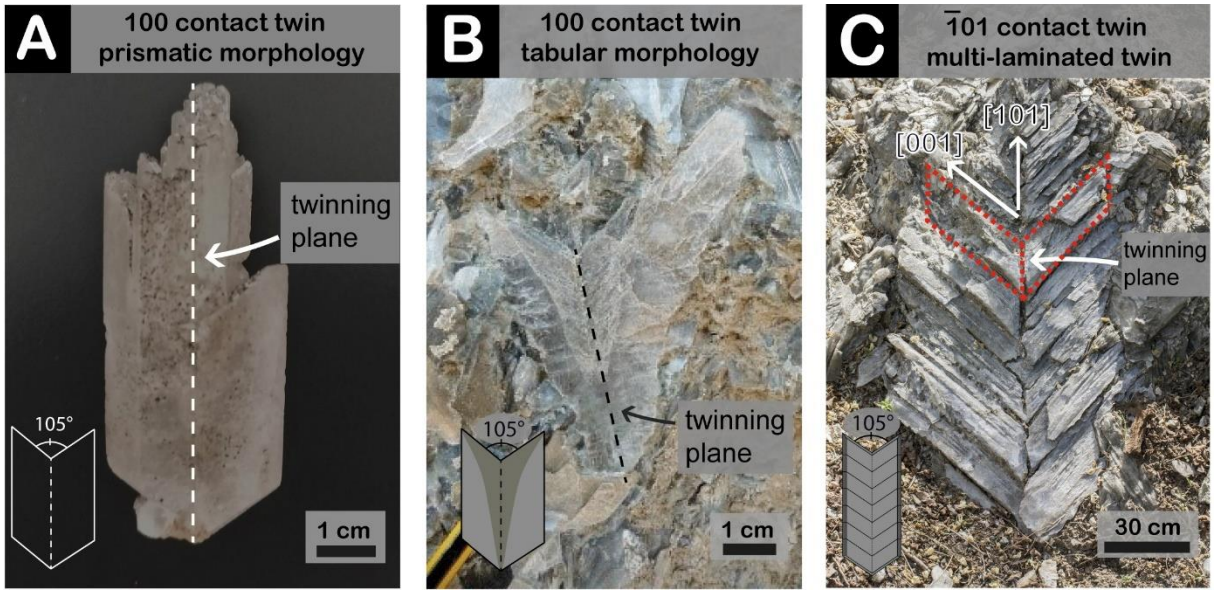

Figure 15 Examples of natural gypsum contact twins in modern and ancient evaporitic environments. A) cm-sized gypsum twin from the Atacama Desert (Chile). B) cm-sized Messinian selenitic gypsum from Piedmont basin (Italy), (courtesy of Marcello Natalicchio). C) meter-sized Messinian selenitic gypsum from "Vena del Gesso Romagnola" (Italy), composed of many sub-crystals obliquely elongated with respect to the twin plane (courtesy of Piero Lucci).

3.3.4. Fluid inclusion directions in $\bar{1}01$ contact twins

Fluid inclusions (FIs) are small droplets of fluid trapped in minerals during their growth from the fluid phase: hence, rapid crystal growth events can result in polyhedric, dendritic or irregular FIs (Roedder, 1984; Bodnar, 2004). However, after trapping, processes of recrystallization generally termed "necking down" start to reduce the high surface energy of the FIs, especially in soluble minerals (Roedder, 1984; Bodnar et al., 1985; Vityk et al., 2000). The final result of such a necking down is the formation of FIs morphologies reflecting those of the host mineral (Goldstein and Reynolds, 1994) at equilibrium with its mother solution, i.e., they represent the negative-equilibrium shape (ES) of the host crystal.

In the 100 gypsum twins, where the two individuals forming the twin grow along [001] direction (Otálora and García-Ruiz, 2014; Costanzo et al., 2019), the primary FIs show a negative-ES elongated along the [001] direction parallel to the twin plane (Goldstein and Reynolds, 1994; Bigi et al., 2022) (Fig. 16A). In contrast, in $\bar{1}01$ twins the [001] direction is oriented obliquely with respect to the twin plane, and thus, FIs negative-ES should develop obliquely with respect to the twin plane as well (Fig. 16B). To assess this hypothesis, optical microscopy has been used to observe FIs in millimetre size gypsum crystals belonging to the $\bar{1}01$ twin law (Fig. 17). The crystal shown in Fig. 17 is one of those synthesized by Krüger et al. (2013). Fig. 17 shows FIs grown along [001] direction, oriented obliquely with respect to the twin plane and the growth direction of the re-entrant angle. Thus, the different orientations of the primary FIs negative-ES with respect to the twin plane is a useful tool to distinguish between the 100 and $\bar{1}01$ twin laws.

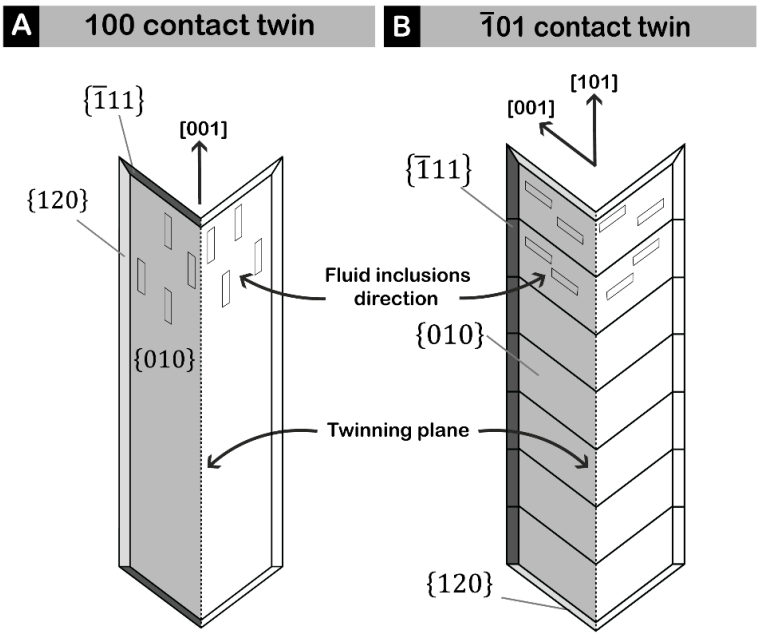

Figure 16 A) The 100 twin law, with fluid inclusions parallel to the twin plane. B) The $\bar{1}01$ twin law, where inclusions are always oriented parallel to [001] direction of single crystals, but obliquely in respect to the twin plane.

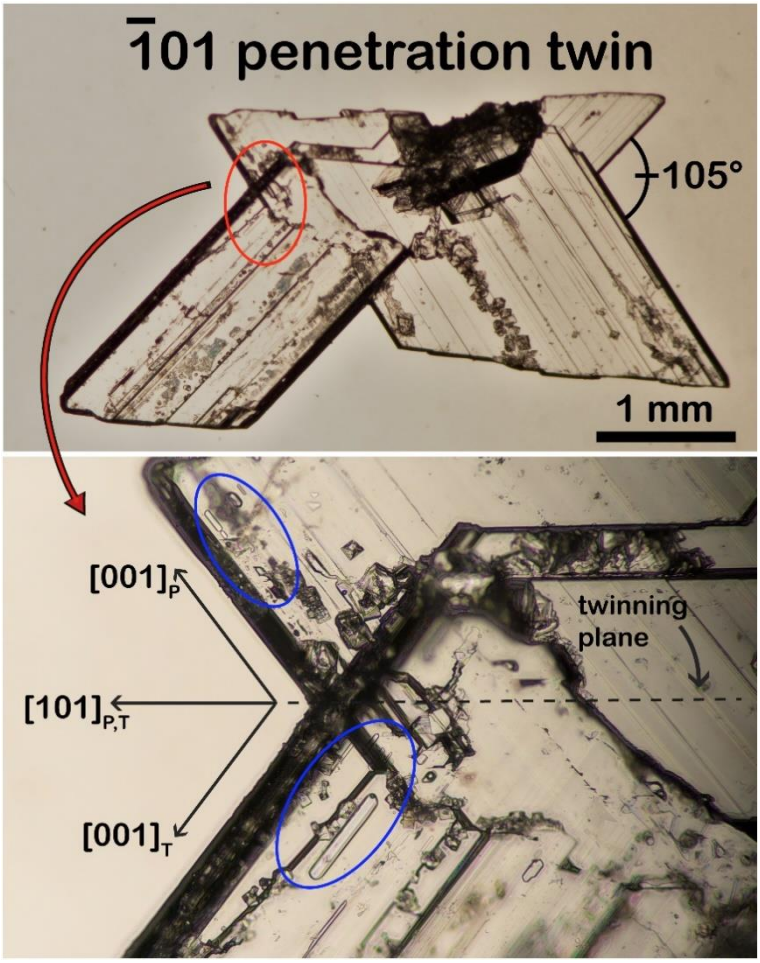

Figure 17 Fluid inclusions in $\bar{1}01$ twins are elongated along [001] and oriented obliquely with respect to the twin plane. Subscripts "P" and "T" identify the two individuals, Parent and Twinned, making the twin.

3.4. Conclusion

In this work, the effect of Ca-carbonate on the gypsum habit was studied by carrying out temperature-controlled laboratory experiments. Starting from two aqueous solutions saturated at 40°C in $CaSO_4{\cdot}2H_2O$ (G1) and in $CaSO_4{\cdot}2H_2O - CaCO_3$ (G2), gypsum has been obtained decreasing the temperature from 40 to 4°C.

We observed that Ca-carbonate triggers the formation of $\bar{1}01$ gypsum contact twins. An epitaxial mechanism between the (100) face of rapidcreekite ($Ca_2SO_4CO_3{\cdot}4H_2O$) and the (010) face of gypsum ($CaSO_4{\cdot}2H_2O$) is suggested to explain the $\bar{1}01$ gypsum contact twin formation. Both the atomic and energetic levels of this mechanism will be discussed in detail in a

forthcoming paper. Furthermore, when comparing the different gypsum twin morphologies observed in evaporitic environments with gypsum twins obtained in our experiments, we claim that the occurrence of $\bar{1}01$ gypsum contact twins in nature is probably more common than considered, and it could be an indicator of high carbonate concentration in brine from which they precipitated. Finally, it has been shown that the different orientation of primary FIs negative-ES with respect to the twin plane, and the main elongation of the sub-crystals making the twin, are a useful tool to distinguish between 100 and $\bar{1}01$ twin laws.

Summing up, the results should help make better use of the twin laws observed in gypsum in ancient sedimentary successions as a proxy for the chemistry of the original brine.

Chapter 4

Growth of gypsum from sulfide-rich solutions in an abiotic oxidizing environment: preliminary results

4.1. Introduction

The 100 gypsum contact twin is a widespread gypsum twin law found in ancient giant saline deposits (the so-called Salt Giants), such as those formed during the middle (Badenian) and late Miocene (Messinian) in the central Paratethys and Mediterranean basins, respectively (e.g., Bąbel, 2004; Ortí, 2010), in response to dramatic evaporitic events (e.g., Hsü, 1972; Peryt, 2006) and for which no modern analogues exist. Intriguingly, in the case of the Mediterranean gypsum deposits, formed during the late Miocene Messinian salinity crisis (e.g., Krijgsman et al., 1999), the precipitation of gypsum by only strictly physical factors (Hsü et al., 1973) is under debate (e.g., Dela Pierre et al., 2015; Carnevale et al., 2019; Pellegrino et al., 2021). Indeed, remains of sulfide-oxidizing bacteria associated with small crystal aggregates of iron sulfide (pyrite), and related polysulfide, have been recognized in the euhedral 100 contact twins observed in the Messinian gypsum deposits (Dela Pierre et al., 2015; Schopf et al., 2012). This discovery has been interpreted as an indication of an active bio-geochemical cycle of sulfur in the solutions from which the gypsum precipitated (Aloisi et al., 2022; Guibourdenche et al., 2022). Thus, in this chapter we raise the question whether the production of H_2S in reducing sedimentary environments and its subsequent oxidation in response to the periodic fluctuation of the redox boundary, might have contributed to the generation of a chemical environment able to induce the precipitation of 100 gypsum contact twins with a growth morphology close to its late Miocene selenitic counterpart. Based on results described in chapter 2, we point out that evaporation alone does not promote the precipitation of 100 contact twins. Moreover, regarding Messinian twinned crystals, the observed 100 contact twins show an unusual twin habit, where the theoretical prismatic habit with sub-crystals parallel to the twin plane (Fig. 5G) is substituted

by a tabular, “swallowtail”, twin habit (Fig. 5H). Hence, some widespread and natural uncommon physico-(bio)-chemical factors, still not understood, promoted this twin habit during the MSC.

Before investigating the effect of the sulfide-oxidizing bacteria on the gypsum habit, it is mandatory to gather preliminary knowledge on the behavior of the abiotic redox pathways of H_2S into SO_4^{2-} and whether it can promote different gypsum habits with respect to those observed in pure solutions. Consequently, in this work we present a simple set of experiments to precipitate gypsum from mixing of gaseous H_2S and $Ca(OH)_2$ solution and by evaporating a Ca^{2+}-SO_4^{2-} rich solution. The objective is to investigate whether impurities related to H_2S oxidation promote different gypsum habits with respect to those observed in pure systems, and especially their twinning. Comparing the results of evaporation experiments in the presence and absence of sulfide oxidation, we argue that the molecules involved in the $H_2S \rightarrow SO_4^{2-}$ oxidation may induce the precipitation of 100 contact twins.

4.2. Materials and Methods

$CaSO_4{\cdot}2H_2O$ reagent plus ($\geq$ 99% Sigma Aldrich), has been used to prepare a $CaSO_4{\cdot}2H_2O$ saturated solution (E1), whereas $Ca(OH)_2$ ACS reagent ($\geq$ 95.0% Sigma Aldrich) has been used to prepare a Ca-rich solution, where H_2S and O_2 have been bubbled, subsequently.

pH measurements have been carried out with a HANNA HI211 pH-meter. Imaging has been performed by optical (Olympus BX4 with JENOPTIC ProgResC5 digital camera), and electron microscopy JEOL-JSM-IT300LV- SEM, equipped with a secondary (SE), backscattered electron (BSE), and an Energy-Dispersive X-Ray spectrometer (EDS). Mineralogical characterization has been performed by a high-resolution confocal μ-Raman system (Horiba Jobin Yvon HR800), equipped with two gratings (1800 and 600 grooves/mm), an air-cooled CCD detector, and a green polarized laser (solid-state Nd, 532 nm, 250 mW).

4.2.1. Experiments

Two sets of crystallization experiments have been carried out (E1, E2), at room temperature (25°C). From the evaporation of the E1 and E2 solutions, single and twinned habits of gypsum crystals have been obtained. The related twin laws have been identified by measuring the extinction angle with the optical microscope using crossed polarizers.

Experiment 1 (E1)

$CaSO_4 \cdot 2H_2O$ saturated solutions have been prepared by adding 0.03 mol/L of $CaSO_4 \cdot 2H_2O_{(s)}$ to water, so exceeding the gypsum saturation in pure water (i.e., ranging from 0.0147 mol/L to 0.0182 mol/L; Lebedev and Kosorukov, 2017). Then, $CaSO_4 \cdot 2H_2O_{(s)}$ has been kept stirring in the flask for 15 days, to ensure saturation. Solution saturation has been verified by conductivity measurements; when the conductivity value does not change significantly, then saturation is reached. We have measured 2220 µS/cm as a stable value. The solution pH was 4.75. Therefore, the solution has been filtered using a cellulose filter with a pore size of 0.45 µm to remove larger $CaSO_4 \cdot 2H_2O$ particles. Then, 30 g of solution have been stored in a 5-cm diameter beaker, covered with a perforated parafilm, and allowed to evaporate at room temperature until about one half of the sample weight. Precipitated crystals have been recovered and washed with ultrapure water, dried overnight at room temperature, and then analyzed by optical and electron microscopy.

Experiment 2 (E2)

The experimental setup is composed as follows (Fig. 18):

I. Two sub-reactors (A and B) to stock and feed the mother solution in the main reactor (C) with the required gases, $H_2S_{(g)}$ and $O_{2(g)}$, produced by the following reactions:

$$FeS_{(s)} + 2HCl_{(aq)} \rightarrow FeCl_{2(aq)} + +H_2S_{(g)} \quad (1)$$

$$2KMnO_{4(s)} + 5H_2O_{2(aq)} + 3H_2SO_{4(aq)} \rightarrow 2MnSO_{4(s)} + 5O_{2(g)} + 8H_2O_{(l)} + K_2SO_{4(aq)} \quad (2)$$

H_2S (sub-reactor A) and O_2 (sub-reactor B) are the reductant and oxidant agents, respectively. In the reaction 1, $FeS_{(s)}$ is the limiting reagent. We used 0.02 mol of $FeS_{(s)}$ in an excess of $HCl_{(aq)}$. Thus, we produced 0.02 mol of $H_2S_{(g)}$. In reaction 2, $KMnO_{4(s)}$ is the limiting reagent. We used 0.02 mol of $KMnO_{4(s)}$ in an excess of $H_2O_{2(aq)}$ and $H_2SO_{4(aq)}$. Thus, we produced 0.05 mol of $O_{2(g)}$.

II. 0.005 mol of $Ca(OH)_2$ have been dissolved in 250 mL of water (i.e., 0.02 mol/L) into the main reactor (C). The solution pH was measured of 12.1. $Ca(OH)_2$ dissolution produces basic pH conditions which enhance H_2S dissociation (Appendix D; Fig. S1). The main reactor is associated with a latex balloon working as expansion tank (D). It allows to briefly store the gases produced by the reactions occurring in A and B. By closing the connections A-C and B-C, we obtained a system where reactions among $Ca(OH)_2$, H_2S, and O_2 can occur. Each gas (O_2 and H_2S) has been bubbled into the main reactor. When O_2 and H_2S enter in the reactor C, H_2S can be oxidized.

In E2, H_2S has been bubbled in C, then the connection A-C has been closed for 24h to allow H_2S dissolution in water. Successively, O_2 has been bubbled following the same procedure. The high amount of $H_2S_{(g)}$, $O_{2(g)}$, and $Ca(OH)_2$ used serves to produce a Ca-sulfate rich solutions supersaturated with respect to gypsum.

After 15 days we stopped the reaction. At this time, the pH of the solution decreased from 12.1 to 6.7 because of the acidic dissociation of H_2S and its oxidation products, such as HSO_2^- and H_2SO_3 (Hoffmann and Lim, 1979). Then, the solution was vacuum filtered using a cellulose filter with a pore size of 0.45 µm. The recovered solid fraction (E2.1) was washed with ultrapure water to remove excess ions, then dried overnight at room temperature and characterized with µ-Raman and SEM techniques. 30 g of the liquid fraction of E2 (i.e., the filtered solution; E2.2) were recovered too, and stored in a 5-cm diameter beaker, covered with a perforated parafilm, and allowed to evaporate at room temperature until about one half of the sample weight.

Precipitated crystals have been recovered and washed with ultrapure water, dried overnight at room temperature, and then analyzed by SEM-EDS.

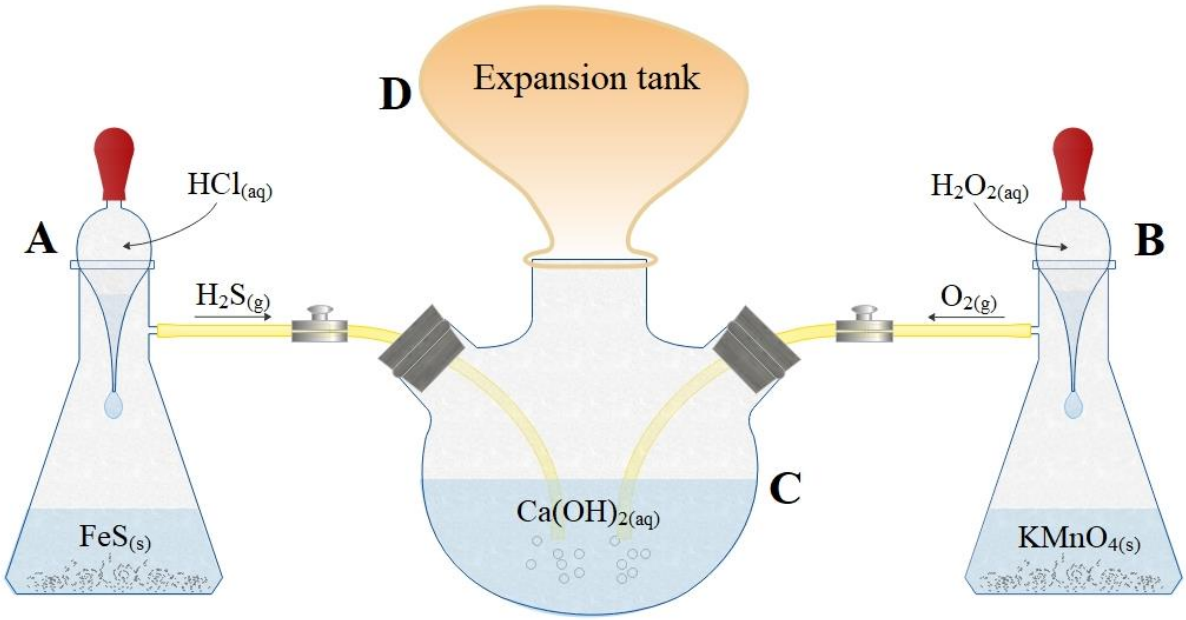

Figure 18 Experimental setup of the reactions E2: $H_2S_{(g)}$ (sub-reactor A) and $O_{2(g)}$ (sub-reactor B) were bubbled into a main reactor (C) containing a calcium rich solution. A latex balloon as expansion tank (D) was exploited as a reservoir of $H_2S_{(g)}$ and $O_{2(g)}$.

4.3. Results and discussions

From the E1 solution (saturated in $CaSO_4 \cdot 2H_2O$) we obtained the precipitation of i) acicular single crystals [001] elongated (Fig. 19A); ii) 100 penetration twins with the two re-entrant angles developing along [001] and [00$\bar{1}$] (Fig. 19B); and iii) $\bar{1}$01 penetration twins with the two re-entrant angles developing along [101] and [$\bar{1}0\bar{1}$] (Fig. 19C). The 100 penetration twin shown in Fig.19A has an aspect ratio of 2.95, whereas the value of 1.40 competes to the $\bar{1}$01 penetration twin in Fig. 19B. These values perfectly agree with the aspect ratio range defined in chapter 2 to discriminate between 100 and $\bar{1}$01 penetration twin laws.

From E2.1 solid fraction, sulfur and gypsum crystals have been identified by means of μ-RS (Appendix D; Fig. S2). However, only anhedral gypsum crystals precipitated, hampering the identification of the crystallographic forms. Thus, the liquid fraction (i.e., the filtered

solution; E2.2) was recovered and allowed to evaporate. Here, gypsum crystals precipitated as an aggregate of twinned crystals. Figure 20 shows gypsum twins with re-entrant angle of 105° and an extinction angle between the two individuals composing the twins of 14° (Appendix D, Fig. S3 for the optical microscopy image). These features allow to identify the 100 twin law. However, the identification of the arrowhead or the two re-entrant angles at the opposite side has been hampered because of the crystal co-precipitation. Nevertheless, in Fig. 20C the two individuals of the twins are in contact, whereas in Fig. 20D they are compenetrated. Thus, 100 twins precipitated in E2.2 may belong both to the contact and penetration growth mechanism, even if the observation of the exact gypsum twin growth morphology is hampered.

The precipitation of 100 contact twins has been observed only in E2.2. Hence, $H_2S \rightarrow SO_4^{2-}$ oxidation is involved in promoting the precipitation of this twin law. However, $H_2S \rightarrow SO_4^{2-}$ oxidation is described through a complex reaction pathway involving different oxidation states of sulfur and, consequently, complex sulfur speciation (e.g., HS^-, S^{2-}, SO_2^{2-}, HSO_2^-, SO_3^{2-}) which can coexist in solution (Hoffmann and Lim, 1979). Thus, it is challenging to identify which specific impurities act as habit modifiers on gypsum crystals without monitoring solution chemistry with specific probes.

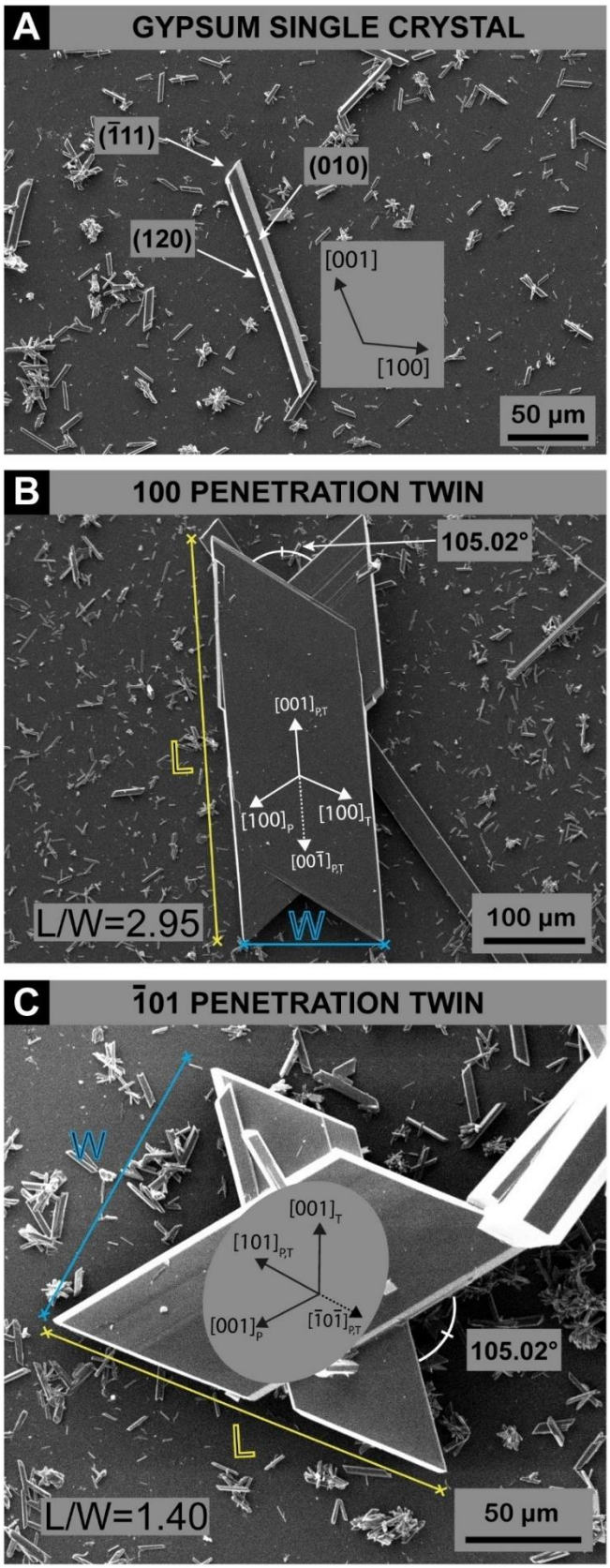

Figure 19 Gypsum crystals precipitated from a pure solution (E1). A) Gypsum single crystals preferentially elongated along [001]. B) 100 penetration twin elongated along [001] direction. C) $\bar{1}01$ penetration twin.

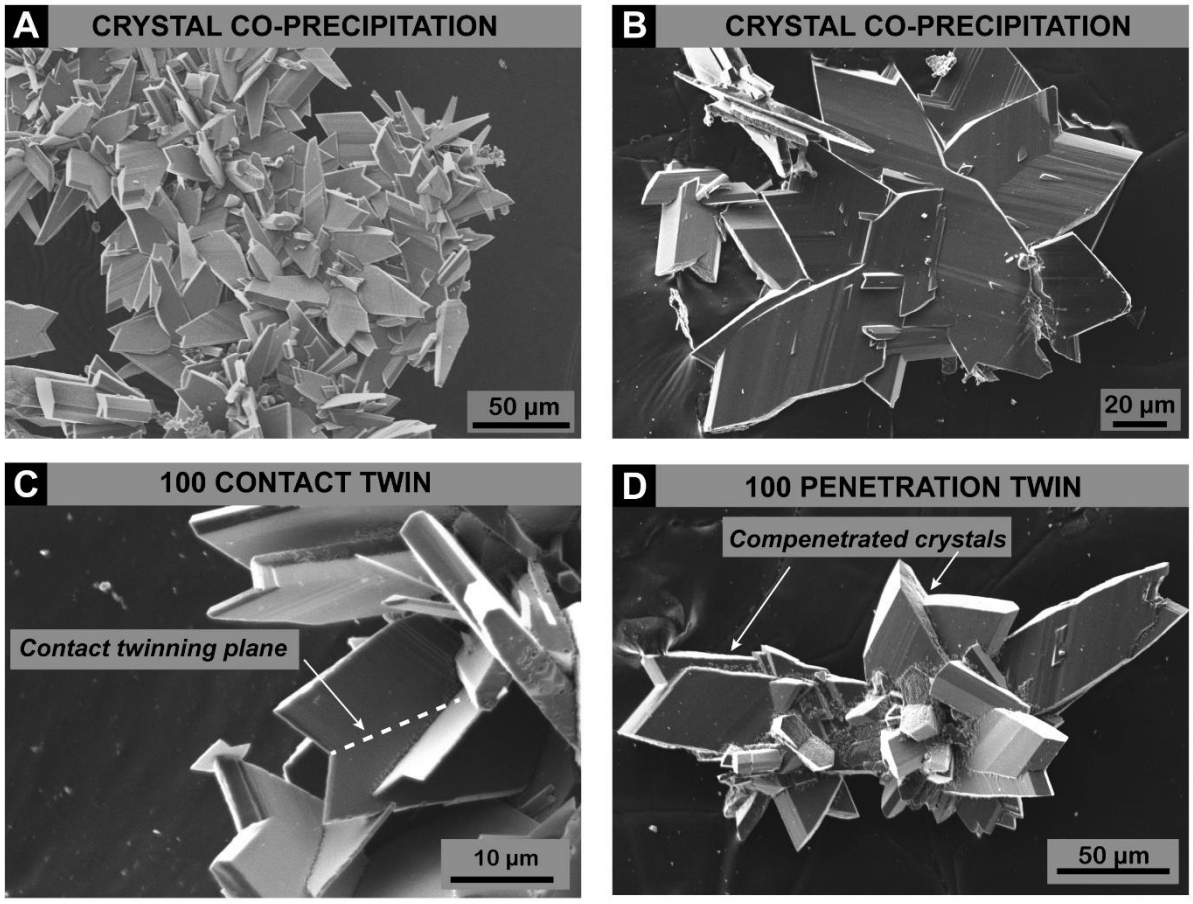

Figure 5 A-B) Extensive co-precipitation of gypsum twins to form aggregates. C) 100 twins with a plausible contact twinning plane D) 100 penetration twin law.

4.4. Conclusions

In this chapter a basic setup is presented to study the growth of gypsum from sulfide-rich waters affected by redox fluctuations resulting from a variable activity of dissolved O_2 and H_2S. This setup is used to perform a few experimental runs and the as-obtained solid products are characterized. Comparing the results of evaporation experiments in the presence and absence of sulfide oxidation we argued that H_2S, along with its oxidation products, may promote the precipitation of 100 gypsum contact twin. These preliminary experimental data seem interesting enough to warrant a deeper study to help in deciphering the link between $H_2S \rightarrow SO_4^{2-}$ redox processes and the formation of 100 gypsum contact twins. However, the data we offered are not conclusive, and as such they do not yet support the notion that sulfide oxidation induces

specific gypsum twinning or habits. Additional data (more experiments) and data analysis (e.g., counting of crystal types) are needed. Moreover, in situ pH and solution speciation analyses of the different experiments should be determined experimentally i) because the concentration of the different species may be critical in promoting different gypsum morphologies; ii) to hypothesize a tentative pathway of $H_2S \rightarrow SO_4^{2-}$ oxidation.

In overall, the experimental design of the study needs to be improved a lot before demonstrating how impurities related to H_2S oxidation control the morphology of gypsum crystals, and specially their twinning. However, the preliminary results of this study may contribute to the debate on the origin of ancient Salt giants, where 100 gypsum contact twins constitute a typical mineral component, providing new experimental data and stimulating further research in the field of the sulfur cycle in sedimentary environments characterized by fluctuating redox conditions.

Summary and concluding remarks

Gypsum ($CaSO_4 \cdot 2H_2O$) is the most abundant natural sulfate mineral on Earth's surface, and it is mostly found in evaporitic environments. The history of Earth, from the Neoproterozoic to the Phanerozoic, was punctuated by remarkable episodes of evaporitic deposition resulted in the accumulation of thick gypsum or anhydrite-bearing sedimentary successions. Furthermore, gypsum deposits have been detected on Mars surface too and a swallowtail gypsum habit, commonly referred to gypsum twins, has been recently observed by the NASA's Curiosity Mars rover. Moreover, gypsum also forms undesired byproducts in many industrial processes, such as desalination. In both natural and industrial environments, gypsum precipitates with different habits, hence, whether the chemical and physical factors producing these habits are understood, these habits i) may provide clues of the depositional environments during growth of gypsum, and ii) may help in designing a new class of additives to provide a precise control over the final habit of gypsum crystals, preventing their adhesion to the surface of equipment, and thus, avoiding blockage of pipe or industrial facilities. Consequently, many chemical and physical variables have been tested as gypsum habit modifiers. Over the last decades, the effect of both inorganic and organic additives was reported as the main parameters affecting gypsum habit, promoting the formation of prismatic, tabular, lenticular, and twinned habits. Nonetheless, twinned gypsum crystals are characterized by an intrinsic morphological variability: five different twin laws are possible for gypsum and each twin law is described by a contact and a penetration twin, hence, at least ten different twinned habits are possible. Despite this theoretical morphological variability, to date the 100 contact twin law is the only well recognized gypsum twin law occurring in natural environments, whereas it has been rarely observed in laboratory experiments where the 100 and $\bar{1}01$ penetration twin laws are the most widespread. Moreover, both field and laboratory publications dealt with the investigation and synthesis of gypsum crystals. Often, twinned crystals have been observed but generally defined

as “swallowtail” twins, so avoiding the twin law’s identification. A limited knowledge on the morphological, crystallographic, and optical characteristics of the five twin laws of gypsum may be at the origin of this missed identification.

The present work fills this gap in knowledge, i) providing a geometric-crystallographic background for the twin law’s identification by means of optical microscopy; ii) univocally identifying the twin laws of gypsum precipitated by evaporation in a pure system; iii) investigating the effect of calcium carbonate ($CaCO_3$) on gypsum growth morphology, paying attention to the twin law identification; iv) presenting preliminary data where an experimental approach has been used to asses condition of precipitation of 100 gypsum contact twins in order to determine the origin of these twins in ancient Salt giants where 100 gypsum contact twins constitute a typical mineral component. Our results indicate that:

I. Different evaporation rates exert a strong morphological control on gypsum crystals. An increase in evaporation rate promotes the precipitation of gypsum crystals (i) with curved habit and (ii) twins according to the 100 and $\overline{1}01$ penetration twin laws, with different precipitation frequencies and habits depending on the evaporation rate. The different crystal aspect ratio (length/width crystal ratio) is proposed as a smart method to discriminate between 100 and $\overline{1}01$ penetration twin laws, and a homo-epitaxial mechanism is invoked to explain the curved habit. Moreover, we suggested i) to consider the evaporation rate as a plausible parameter in promoting the curved habit in natural environment, overall, the evaporitic one, and ii) the occurrence of 100 and $\overline{1}01$ penetration twin laws in sedimentary environments.

II. Carbonate ions in solution trigger the formation of $\overline{1}01$ gypsum contact twins. An epitaxial mechanism between the (100) face of rapidcreekite ($Ca_2SO_4CO_3 \cdot 4H_2O$) and the (010) face of gypsum ($CaSO_4 \cdot 2H_2O$) is suggested to explain the $\overline{1}01$ gypsum contact twin formation. This is the first evidence of the effect of Ca-carbonate as a

specific impurity promoting the formation of the $\overline{1}01$ contact twin law. Moreover, we compared the natural gypsum twin morphologies observed in evaporitic environments with those obtained in our experiments and suggested the occurrence of $\overline{1}01$ gypsum contact twins in nature. We claimed that the occurrence of $\overline{1}01$ gypsum contact twins in nature is higher than that considered today, and it could be an indicator of high carbonate concentration in brine from which they precipitated. Finally, it has been shown that the different orientation of primary fluid inclusions (of the negative crystal-shaped) with respect to the twin plane, and the main elongation of the sub-crystals making the twin, is a useful tool to distinguish between 100 and $\overline{1}01$ twin laws, whose geometry is otherwise very hard to distinguish especially in rock samples.

III. The overall chemical species resulting from H_2S oxidation in solution may be involved in triggering the precipitation of 100 contact twins, i.e., the most widespread gypsum twin found in ancient sedimentary successions.

To summarize, our results improve the knowledge of the influences of variations in solution composition on the habits of gypsum crystals. This may aid understanding the chemistry of the original brine in ancient sedimentary successions depending on the twin law of gypsum observed and their habit.

References

Akyol, E., Öner, M., Barouda, E., Demadis, K.D. (2009). Systematic Structural Determinants of the Effects of Tetraphosphonates on Gypsum Crystallization. *Crystal growth & design, 9*(12), 5145–5154. https://doi.org/10.1021/cg9005423.

Aloisi, G., Guibourdenche, L., Natalicchio, M., Caruso, A., Haffert, L., El Kilany, A., Dela Pierre, F. (2022). The geochemical riddle of "low-salinity gypsum" deposits. *Geochimica et Cosmochimica Acta, 327*, 247-275, https://doi.org/10.1016/j.gca.2022.03.033.

Aquilano, D., Otálora, F., Pastero, L., García-Ruiz, J.M. (2016). Three study cases of growth morphology in minerals: Halite, calcite and gypsum. *Progress in Crystal Growth and Characterization of Materials, 62*(2), 227–251, https://doi.org/10.1016/j.pcrysgrow.2016.04.012.

Aquilano, D., Rubbo, M., Catti, M., Pavese, A. (1997). Theoretical equilibrium and growth morphology of $CaCO_3$ polymorphs. I. Aragonite. *Journal of crystal growth, 182*(1-2), 168–184. https://doi.org/10.1016/S0022-0248(97)00334-5.

Avdontceva, M.S., Zolotarev, A.A., Krivovichev, S.V., Krzhizhanovskaya, M.G., Bocharov, V.N., Shilovskikh, V.V., Zolotarev, A.A., Rassomakhin, M.A. (2021). Rapidcreekite of anthropogenic origin - 'korkinoite' from burnt mine dump in the Chelyabinsk coal basin, South Urals, Russia: crystal structure refinement, thermal behavior and spectroscopic characterization. *Journal of Geosciences, 66*(3), 147-156. https://doi.org/10.3190/jgeosci.327.

Bąbel, M. (2004). Models for evaporite, selenite and gypsum microbialite deposition in ancient saline basins. *Acta Geologica Polonica, 54*(2), 219-249.

Bąbel, M., Becker, A. (2006). Cyclonic Brine-Flow Pattern Recorded by Oriented Gypsum Crystals in the Badenian Evaporite Basin of the Northern Carpathian Foredeep. *Journal of Sedimentary Research, 76*(7), 996-1011. https://doi.org/10.2110/jsr.2006.090.

Bąbel, M., Olszewska-Nejbert, D., Nejbert, K., Ługowski, D. (2015). The Badenian evaporative stage of the Polish Carpathian Foredeep: sedimentary facies and depositional environment of the selenitic Nida Gypsum succession. In *Guidebook for field trips accompanying IAS 31st Meeting of Sedimentology held in Kraków on 22nd–25th of June* (pp. 25-50).

Badino, G., Chignola, R. (2019). Fluctuations of Atmospheric Pressure and the Sound of Underground Karst Systems: The Antro del Corchia Case (Apuane Alps, Italy). *Frontiers in Earth Science, 7,* 147. https://doi.org/10.3389/feart.2019.00147.

Bigi, D., Lugli, S., Manzi, V., Roveri, M. (2022). Are fluid inclusions in gypsum reliable paleoenvironmental indicators? An assessment of the evidence from the Messinian evaporites. *Geology, 50*(4), 454–459. https://doi.org/10.1130/G49475.1.

Bodnar, R. (2004). Reequilibration of fluid inclusions. *Fluid inclusions: Analysis and interpretation*, *32*, 213-230. https://doi.org/10.1007/s00126-004-0411-6.

Bodnar, R.J., Reynolds, T.J., Kuehn, C.A. (1985). Fluid-Inclusion Systematics in Epithermal Systems. https://doi.org/10.5382/Rev.02.05.

Boeyens, J.C.A., Ichharam, V.V.H. (2002). Redetermination of the crystal structure of calcium sulphate dihydrate, $CaSO_4 \cdot 2H_2O$. *Zeitschrift für Kristallographie-new crystal structures*, *217*(JG), 9-10. https://doi.org/10.1524/ncrs.2002.217.1.9.

Bots, P. (2011). *Experimental investigation of calcium carbonate mineralogy in past and future oceans*. PhD thesis, University of Leeds. ISBN 978-0-85731-160-3.

Bruno, M., Massaro, F.R., Pastero, L., Costa, E., Rubbo, M., Prencipe, M., Aquilano, D. (2013). New Estimates of the Free Energy of Calcite/Water Interfaces for Evaluating the Equilibrium Shape and Nucleation Mechanisms. *Crystal growth & design*, *13*(3), 1170-1179. https://doi.org/10.1021/cg3015817.

Bruno, M., Pastero, L., Cotellucci, A., Aquilano, D., (2022a). Epitaxy: a methodological approach to the study of an old phenomenon. *CrystEngComm*, *24*(23), 4165-4173. https://doi.org/10.1039/d2ce00340f.

Bruno, M., Prencipe, M., Aquilano, D., Cotellucci, A., Ghignone, S., Németh, P., (2022b). Calcite/Aragonite Epitaxy: A Computational Study for Understanding Mollusk Shell Formation. *The Journal of Physical Chemistry C*, *126*(14), 6472-6481. https://doi.org/10.1021/acs.jpcc.2c00785.

Budz, J., Jones, A.G., Mullin, J.W. (1986). Effect of selected impurities on the continuous precipitation of calcium sulphate (gypsum). *Journal of Chemical Technology & Biotechnology*, *36*(4), 153-161. https://doi.org/10.1002/jctb.280360402.

Canals, À., Van Driessche, A.E.S., Palero, F., García-Ruiz, J.M. (2019). The origin of large gypsum crystals in the Geode of Pulpí (Almería, Spain). *Geology 47*(12), 1161–1165. https://doi.org/10.1130/G46734.1.

Carnevale, G., Gennari, R., Lozar, F., Natalicchio, M., Pellegrino, L., Dela Pierre, F. (2019). Living in a deep desiccated Mediterranean Sea: An overview of the Italian fossil record

of the Messinian salinity crisis. *Bollettino della Società Paleontologica Italiana*, *58*, 109-140.

Cody, A. M., Cody, R. D. (1989a). SEM and polarization analyses updating early light microscope studies related to {101} twin formation in gypsum. *Journal of crystal growth*, *98*(4), 731-738. https://doi.org/10.1016/0022-0248(89)90311-4.

Cody, A. M., Cody, R. D. (1989b). Evidence for micro-biological induction of {101} montmartre twinning of gypsum ($CaSO4 \cdot 2H_2O$). *Journal of crystal growth, 98*(4), 721-730. https://doi.org/10.1016/0022-0248(89)90310-2.

Cody, R. D. (1979). Lenticular gypsum; occurrences in nature, and experimental determinations of effects of soluble green plant material on its formation. *Journal of Sedimentary Research, 49*(3), 1015-1028. https://doi.org/10.1306/212f78a6-2b24-11d7-8648000102c1865d.

Cody, R. D. (1976). Growth and early diagenetic changes in artificial gypsum crystals grown within bentonite muds and gels. *Geological Society of America Bulletin*, *87*(8), 1163-1168. https://doi.org/10.1130/0016-7606(1976)87<1163:gaedci>2.0.co;2.

Cody, R. D., Cody, A. M. (1988). Gypsum nucleation and crystal morphology in analog saline terrestrial environments. *Journal of Sedimentary Research*, *58*(2), 247-255. https://doi.org/10.1306/212f8d69-2b24-11d7-8648000102c1865d.

Cole, W. F., Lancucki, C. J. (1974). A refinement of the crystal structure of gypsum $CaSO_4 \cdot 2H_2O$. *Acta Crystallographica Section B: Structural Crystallography and Crystal Chemistry*, *30*(4), 921-929. https://doi.org/10.1107/s0567740874004055.

Cooper, M. A., Hawthorne, F. C. (1996). The crystal structure of rapidcreekite, $Ca_2(SO_4)(CO_3)(H_2O)_4$, and its relation to the structure of gypsum. *The Canadian Mineralogist*, *34*(1), 99-106.DOI

Costanzo, A., Cipriani, M., Feely, M., Cianflone, G., Dominici, R. (2019). Messinian twinned selenite from the Catanzaro Trough, Calabria, Southern Italy: field, petrographic and fluid inclusion perspectives. *Carbonates and Evaporites*, *34*, 743-756. https://doi.org/10.1007/s13146-019-00516-0.

Cotellucci, A., Otálora, F., Canals, A., Criado-Reyes, J., Pellegrino, L., Bruno, M., ... & Pastero, L. (2023a). $\bar{1}01$ contact twins in gypsum experimentally obtained from calcium carbonate enriched solutions: mineralogical implications for natural gypsum deposits. *Journal of Applied Crystallography*, *56*(3). https://doi.org/10.1107/s1600576723002674.

Cotellucci, A., Pellegrino, L., Costa, E., Bruno, M., Pierre, F. D., Aquilano, D., ... & Pastero, L. (2023b). Effect of Different Evaporation Rates on Gypsum Habit: Mineralogical Implications for Natural Gypsum Deposits. *Crystal Growth & Design*. https://doi.org/10.1021/acs.cgd.3c01124.

Coto, B., Martos, C., Peña, J. L., Rodríguez, R., Pastor, G. (2012). Effects in the solubility of $CaCO_3$: Experimental study and model description. *Fluid Phase Equilibria*, *324*, 1-7. https://doi.org/10.1016/j.fluid.2012.03.020.

Craker, W. E., & Schiller, K. K. (1962). Plastic deformation of gypsum. *Nature*, *193*(4816), 672-673. https://doi.org/10.1038/193672a0.

Criado-Reyes, J., Pastero, L., Bruno, M., García-Ruiz, J. M., Aquilano, D., & Otálora, F. (2020). Equilibrium Shape of 2D Nuclei Obtained from Spiral Hillocks on {010} Form of Gypsum. *Crystal Growth & Design*, *20*(3), 1526-1530. https://doi.org/10.1021/acs.cgd.9b01246.

Dana, J. D. (1864). *Manual of Mineralogy*, Wiley.

De Vreugd, C. H., Witkamp, G. J., & Van Rosmalen, G. M. (1994). Growth of gypsum III. Influence and incorporation of lanthanide and chromium ions. *Journal of crystal growth*, *144*(1-2), 70-78. https://doi.org/10.1016/0022-0248(94)90012-4.

Dela Pierre, F., Natalicchio, M., Ferrando, S., Giustetto, R., Birgel, D., Carnevale, G., ... & Peckmann, J. (2015). Are the large filamentous microfossils preserved in Messinian gypsum colorless sulfide-oxidizing bacteria?. *Geology*, *43*(10), 855-858. https://doi.org/10.1130/g37018.1.

Dhanaraj, G., Byrappa, K., Prasad, V., & Dudley, M. (Eds.). (2010). *Springer Handbook of Crystal Growth.* Springer Berlin Heidelberg. https://doi.org/10.1007/978-3-540-74761-1.

Engel, A. S., Stern, L. A., & Bennett, P. C. (2004). Microbial contributions to cave formation: new insights into sulfuric acid speleogenesis. *Geology*, *32*(5), 369-372. https://doi.org/10.1130/G20288.1

Follner, S., Wolter, A., Helming, K., Silber, C., Bartels, H., & Follner, H. (2002). On the real structure of gypsum crystals. *Crystal Research and Technology: Journal of Experimental and Industrial Crystallography*, *37*(2-3), 207-218. https://doi.org/10.1002/1521-4079(200202)37:2/3<207::aid-crat207>3.0.co;2-l.

García-Ruiz, J. M., Villasuso, R., Ayora, C., Canals, A., & Otálora, F. (2007). Formation of natural gypsum megacrystals in Naica, Mexico. *Geology*, *35*(4), 327-330. https://doi.org/10.1130/g23393a.1.

Germano Rigault, 2005. Introduzione alla cristallografia. Levrotto&Bella.

Goldstein, R. H., & Reynolds, T. J. (1994). *Systematics of fluid inclusions in diagenetic minerals*. SEPM Society for Sedimentary Geology. https://doi.org/10.2110/scn.94.31.

Gomell, A. K., & Pflitsch, A. (2022). Airflow dynamics in Wind Cave and Jewel Cave: How do barometric caves breathe?. *International Journal of Speleology*, *51*(3), 1. https://doi.org/10.5038/1827-806x.51.3.2437.

Guibourdenche, L., Cartigny, P., Pierre, F. D., Natalicchio, M., & Aloisi, G. (2022). Cryptic sulfur cycling during the formation of giant gypsum deposits. *Earth and Planetary Science Letters*, *593*, 117676. https://doi.org/10.1016/j.epsl.2022.117676.

Hartman, P., & Perdok, W. G. (1955a). On the relations between structure and morphology of crystals. I. *Acta Crystallographica*, *8*(1), 49-52. https://doi.org/10.1107/S0365110X55000121.

Hartman, P., & Perdok, W. G. (1955b). On the relations between structure and morphology of crystals. II. *Acta Crystallographica*, *8*(9), 521-524. https://doi.org/10.1107/S0365110X55001679.

Hartman, P. P. W. G., & Perdok, W. G. (1955c). On the relations between structure and morphology of crystals. III. *Acta Crystallographica*, *8*(9), 525-529. https://doi.org/10.1107/S0365110X55001680.

Heijnen, W. M. M., & Hartman, P. (1991). Structural morphology of gypsum ($CaSO_4$ $2H_2O$), brushite ($CaHPO_4$ $2H_2O$) and pharmacolite ($CaHAsO_4$ $2H_2O$). *Journal of Crystal Growth*, *108*(1-2), 290-300. https://doi.org/10.1016/0022-0248(91)90376-G.

Hoffmann, M. R., & Lim, B. C. (1979). Kinetics and mechanism of the oxidation of sulfide by oxygen: catalysis by homogeneous metal-phthalocyanine complexes. *Environmental Science & Technology*, *13*(11), 1406-1414. https://doi.org/10.1021/es60159a014.

Hsü, K. J. (1972). Origin of saline giants: a critical review after the discovery of the Mediterranean evaporite. *Earth-Science Reviews*, *8*(4), 371-396. https://doi.org/10.1016/0012-8252(72)90062-1.

Hsü, K. J., Ryan, W. B., & Cita, M. B. (1973). Late Miocene desiccation of the Mediterranean. *Nature*, *242*(5395), 240-244. https://doi.org/10.1038/242240a0.

Jafarzadeh, A. A., & Burnham, C. P. (1992). Gypsum crystals in soils. *Journal of soil science*, *43*(3), 409-420. https://doi.org/10.1111/j.1365-2389.1992.tb00147.x.

de Jong, W. F., & Bouman, J. (1939). Das reziproke und das Bravaissche Gitter von Gips. *Zeitschrift für Kristallographie-crystalline materials*, *100*(1-6), 275-276. https://doi.org/10.1524/zkri.1939.100.1.275.

Kellermeier, M., Cölfen, H., & García-Ruiz, J. M. (2012). Silica biomorphs: Complex biomimetic hybrid materials from "sand and chalk". *European Journal of Inorganic Chemistry*, *2012*(32), 5123-5144. https://doi.org/10.1002/ejic.201201029.

Kern, R., Rehn, B. (1960). Etude experimentale de la formation des macles de croissance du gypse. *Comptes Rendus Hebdomadaires des Séances de l'Academie des Sciences. 251*, 1300–1302.

Khalkhali, M., Ma, X., Zhang, H., & Liu, Q. (2019). Bulk and surface properties of gypsum: A comparison between classical force fields and dispersion-corrected DFT calculations. *Computational Materials Science*, *164*, 8-16. https://doi.org/10.1016/j.commatsci.2019.03.045.

Klein, C., Hurlbut, C.S., Dana, J.D. (1993). Hurlbut Jr, Wiley, New York. Manual of mineralogy. ISBN 0471535605. *Geological Journal, 30*(1), 84–85. Portico. https://doi.org/10.1002/gj.3350300114.

Krijgsman, W., Hilgen, F. J., Raffi, I., Sierro, F. J., & Wilson, D. S. (1999). Chronology, causes and progression of the Messinian salinity crisis. *Nature*, *400*(6745), 652-655. https://doi.org/10.1038/23231.

Krüger, Y., García-Ruiz, J. M., Canals, À., Marti, D., Frenz, M., & Van Driessche, A. E. (2013). Determining gypsum growth temperatures using monophase fluid inclusions—Application to the giant gypsum crystals of Naica, Mexico. *Geology*, *41*(2), 119-122. https://doi.org/10.1130/G33581.1.

Lacroix, A. (1893). *Minéralogie de la France et de ses colonies : description physique et chimique des minéraux, étude des conditions géologiques de leurs gisements,* (Vol. 2). Baudry. https://doi.org/10.5962/bhl.title.130458.

Lebedev, A. L., & Kosorukov, V. L. (2017). Gypsum solubility in water at 25 °C. *Geochemistry International*, *55*, 205-210.. https://doi.org/10.1134/S0016702917010062.

Massaro, F. R., Rubbo, M., & Aquilano, D. (2010). Theoretical equilibrium morphology of gypsum ($CaSO_4$ $2H_2O$). 1. A syncretic strategy to calculate the morphology of crystals. *Crystal Growth & Design*, *10*(7), 2870-2878. https://doi.org/10.1021/cg900660v.

Massaro, F. R., Rubbo, M., & Aquilano, D. (2011). Theoretical equilibrium morphology of gypsum ($CaSO_4$ $2H_2O$). 2. The stepped faces of the main [001] zone. *Crystal growth & design*, *11*(5), 1607-1614. https://doi.org/10.1021/cg101570c.

Mbogoro, M. M., Peruffo, M., Adobes-Vidal, M., Field, E. L., O'Connell, M. A., & Unwin, P. R. (2017). Quantitative 3D visualization of the growth of individual gypsum microcrystals: Effect of Ca^{2+}:SO_4^{2-} ratio on kinetics and crystal morphology. *The Journal of Physical Chemistry C*, *121*(23), 12726-12734. https://doi.org/10.1021/acs.jpcc.7b01566.

Mees, F., Casteneda, C., Herrero, J., & Van Ranst, E. (2012). The nature and significance of variations in gypsum crystal morphology in dry lake basins. *Journal of Sedimentary Research*, *82*(1), 37-52. https://doi.org/10.2110/jsr.2012.3.

Montagnino, D., Costa, E., Massaro, F. R., Artioli, G., & Aquilano, D. (2011). Growth morphology of gypsum in the presence of copolymers. *Crystal Research and Technology*, *46*(10), 1010-1018.https://doi.org/10.1002/crat.201100131.

Morales, J., Astilleros, J. M., Matesanz, E., & Fernández-Díaz, L. (2016). The growth of gypsum in the presence of hexavalent chromium: A multiscale study. *Minerals*, *6*(1), 22. https://doi.org/10.3390/min6010022.

Mutaftschiev, B., & Mutaftschiev, B. (2001). *The atomistic nature of crystal growth* (Vol. 43). Berlin: Springer. https://doi.org/10.1007/978-3-662-04591-6.

Natalicchio, M., Birgel, D., Dela Pierre, F., Ziegenbalg, S., Hoffmann-Sell, L., Gier, S., & Peckmann, J. (2022). Messinian bottom-grown selenitic gypsum: An archive of microbial life. *Geobiology*, *20*(1), 3-21. https://doi.org/10.1111/gbi.12464.

Natalicchio, M., Pellegrino, L., Clari, P., Pastero, L., & Pierre, F. D. (2021). Gypsum lithofacies and stratigraphic architecture of a Messinian marginal basin (Piedmont Basin, NW Italy). *Sedimentary Geology*, *425*, 106009. https://doi.org/10.1016/j.sedgeo.2021.106009.

Nespolo, M., & Ferraris, G. (2004). The oriented attachment mechanism in the formation of twins-a survey. *European Journal of Mineralogy*, *16*(3), 401-406. https://doi.org/10.1127/0935-1221/2004/0016-0401.

Nesse, W.D., 2012. Introduction to mineralogy, 2. ed. ed. Oxford Univ. Press, New York, NY. ISBN 0-19-510691-l. *Mineralogical Magazine, 64*(5), 966-967. doi:10.1180/S0026461X00026608.

Ortí, F. (2010). Selenite facies in marine evaporites: a review. *Quaternary Carbonate and Evaporite Sedimentary Facies and Their Ancient Analogues*, 431–463. Portico. https://doi.org/10.1002/9781444392326.ch20.

Otálora, F., & García-Ruiz, J. (2014). Nucleation and growth of the Naica giant gypsum crystals. *Chemical Society Reviews*, *43*(7), 2013-2026. https://doi.org/10.1039/C3CS60320B

Panczner, W. D. (1987). *Minerals of Mexico*. Springer US. https://doi.org/10.1007/978-1-4757-5848-1.

Parkhurst, D. L., & Appelo, C. A. J. (2013). Description of input and examples for PHREEQC version 3: a computer program for speciation, batch-reaction, one-dimensional transport, and inverse geochemical calculations. *Techniques and Methods 6*(A43), 497. https://doi.org/10.3133/tm6a43.

Parsons, S. (2003). Introduction to twinning. *Acta Crystallographica Section D: Biological Crystallography*, *59*(11), 1995-2003. https://doi.org/10.1107/S0907444903017657.

Pedersen, B. F., & Semmingsen, D. (1982). Neutron diffraction refinement of the structure of gypsum, $CaSO_4$. $2H_2O$. *Acta Crystallographica Section B: Structural Crystallography and Crystal Chemistry*, *38*(4), 1074-1077. https://doi.org/10.1107/S0567740882004993

Pellegrino, L., Natalicchio, M., Abe, K., Jordan, R. W., Longo, S. E. F., Ferrando, S., ... & Pierre, F. D. (2021). Tiny, glassy, and rapidly trapped: The nano-sized planktic diatoms in Messinian (late Miocene) gypsum. *Geology*, *49*(11), 1369-1374. https://doi.org/10.1130/G49342.1.

Peryt, T. M. (2006). The beginning, development and termination of the Middle Miocene Badenian salinity crisis in Central Paratethys. *Sedimentary Geology*, *188*, 379-396. https://doi.org/10.1016/j.sedgeo.2006.03.014.

Pinto, A. J., Ruiz-Agudo, E., Putnis, C. V., Putnis, A., Jiménez, A., & Prieto, M. (2010). AFM study of the epitaxial growth of brushite ($CaHPO_4$ $2H_2O$) on gypsum cleavage surfaces. *American Mineralogist*, *95*(11-12), 1747-1757. https://doi.org/10.2138/am.2010.3557.

Plummer, N. L., & Busenberg, E. (1982). The solubilities of calcite, aragonite and vaterite in CO_2-H_2O solutions between 0 and 90° C, and an evaluation of the aqueous model for the system $CaCO_3$-CO_2-H_2O. *Geochimica et Cosmochimica Acta*, *46*, 1011-1040. https://doi.org/10.1016/0016-7037(82)90056-4.

Popov, K., Rudakova, G., Larchenko, V., Tusheva, M., Kamagurov, S., Dikareva, J., & Kovaleva, N. (2016). A comparative performance evaluation of some novel “green” and traditional antiscalants in calcium sulfate scaling. *Advances in Materials Science and Engineering*, *2016*. https://doi.org/10.1155/2016/7635329.

Prisciandaro, M., Lancia, A., & Musmarra, D. (2022). Gypsum scale control by phosphonate additives. In *Water-Formed Deposits*. Elsevier. https://doi.org/10.1016/B978-0-12-822896-8.00030-3.

Punin, Y. O., & Artamonova, O. I. (2001). Autodeformation bending of gypsum crystals grown under the conditions of counterdiffusion. *Crystallography Reports*, *46*, 138-143. https://doi.org/10.1134/1.1343142.

Rabizadeh, T., Morgan, D. J., Peacock, C. L., & Benning, L. G. (2019). Effectiveness of green additives vs poly (acrylic acid) in inhibiting calcium sulfate dihydrate crystallization. *Industrial & Engineering Chemistry Research*, *58*(4), 1561-1569. https://doi.org/10.1021/acs.iecr.8b02904.

Rabizadeh, T., Peacock, C. L., & Benning, L. G. (2020). Investigating the effectiveness of phosphonate additives in hindering the calcium sulfate dihydrate scale formation. *Industrial & Engineering Chemistry Research*, *59*(33), 14970-14980. https://doi.org/10.1021/acs.iecr.0c03600.

Rabizadeh, T., Peacock, C. L., & Benning, L. G. (2014). Carboxylic acids: effective inhibitors for calcium sulfate precipitation?. *Mineralogical Magazine*, *78*(6), 1465-1472. https://doi.org/10.1180/minmag.2014.078.6.13.

Rabizadeh, T., Stawski, T. M., Morgan, D. J., Peacock, C. L., & Benning, L. G. (2017). The effects of inorganic additives on the nucleation and growth kinetics of calcium sulfate dihydrate crystals. *Crystal Growth & Design*, *17*(2), 582-589. https://doi.org/10.1021/acs.cgd.6b01441.

Ramírez-García, P., Duran-Olivencia, M. A., Kellermeier, M., & Van Driessche, A. E. (2022). Determining the operational window of green antiscalants: A case study for calcium sulfate. *Desalination*, *544*, 116128. https://doi.org/10.1016/j.desal.2022.116128.

Reid, R. P., Oehlert, A. M., Suosaari, E. P., Demergasso, C., Chong, G., Escudero, L. V., ... & Palma, A. T. (2021). Electrical conductivity as a driver of biological and geological spatial heterogeneity in the Puquios, Salar de Llamara, Atacama Desert, Chile. *Scientific reports*, *11*(1), 12769. https://doi.org/10.1038/s41598-021-92105-2.

Reiss, A. G., Ganor, J., & Gavrieli, I. (2019). Size distribution and morphology of gypsum crystals precipitating from hypersaline solutions. *Crystal Growth & Design*, *19*(12), 6954-6962. https://doi.org/10.1021/acs.cgd.9b00735.

Reiss, A. G., Gavrieli, I., & Ganor, J. (2020). The effect of phosphonate-based antiscalant on gypsum precipitation kinetics and habit in hyper-saline solutions: An experimental and

modeling approach to the planned Red Sea–Dead Sea Project. *Desalination*, *496*, 114638. https://doi.org/10.1016/j.desal.2020.114638.

Reiss, A. G., Gavrieli, I., Rosenberg, Y. O., Reznik, I. J., Luttge, A., Emmanuel, S., & Ganor, J. (2021). Gypsum precipitation under saline conditions: thermodynamics, kinetics, morphology, and size distribution. *Minerals*, *11*(2), 141. https://doi.org/10.3390/min11020141.

Rinaudo, C., Franchini-Angela, M., & Boistelle, R. (1989). Curvature of gypsum crystals induced by growth in the presence of impurities. *Mineralogical Magazine*, *53*(372), 479-482. https://doi.org/10.1180/minmag.1989.053.372.08.

Rinaudo, C., Robert, M. C., & Lefaucheux, F. (1985). Growth and characterization of gypsum crystals. *Journal of crystal growth*, *71*(3), 803-806. https://doi.org/10.1016/0022-0248(85)90396-3.

Roberts, A. C., Ansell, H. G., Jonasson, I. R., Grice, J. D., & Ramik, R. A. (1986). Rapidcreekite, a new hydrated calcium sulfate-carbonate from the Rapid Creek area, Yukon Territory. *The Canadian Mineralogist*, *24*(1), 51-54.

Rodríguez-Aranda, J. P., Rouchy, J. M., Calvo, J. P., Ordóñez, S., & del Cura, M. G. (1995). Unusual twinning features in large primary gypsum crystals formed in salt lake conditions, Middle Miocene, Madrid Basin, Spain—paleoenvironmental implications. *Sedimentary Geology*, *95*(1-2), 123-132. https://doi.org/10.1016/0037-0738(94)00103-2.

Rodríguez-Blanco, J. D., Jiménez, A., & Prieto, M. (2007). Oriented Overgrowth of Pharmacolite ($CaHAsO_4 \cdot 2H_2O$) on Gypsum ($CaSO_4 \cdot 2H_2O$). *Crystal Growth & Design*, 7(12), 2756–2763. https://doi.org/10.1021/cg070222+.

Roedder, E. (1984). Fluid inclusions. *Reviews in mineralogy*, *12*, 644. https://doi.org/10.1515/9781501508271.

Rosenberg, Y. O., Reznik, I. J., Zmora-Nahum, S., & Ganor, J. (2012). The effect of pH on the formation of a gypsum scale in the presence of a phosphonate antiscalant. *Desalination*, *284*, 207-220. https://doi.org/10.1016/j.desal.2011.08.061.

Rubbo, M., Bruno, M., Massaro, F. R., & Aquilano, D. (2012a). The Five Twin Laws of Gypsum ($CaSO_4 \cdot 2H_2O$): A Theoretical Comparison of the Interfaces of the Contact Twins. *Crystal Growth & Design*, 12(1), 264–270. https://doi.org/10.1021/cg201031s

Rubbo, M., Bruno, M., Massaro, F. R., & Aquilano, D. (2012b). The Five Twin Laws of Gypsum ($CaSO_4 \cdot 2H_2O$): A Theoretical Comparison of the Interfaces of the Penetration

Twins. *Crystal Growth & Design*, 12(6), 3018–3024. https://doi.org/10.1021/cg300227j.

Rubbo, M., Massaro, F. R., Aquilano, D., & Vanzetti, W. (2011). Morphology of gypsum: a case study. *Crystal Research and Technology*, *46*(8), 779-783. https://doi.org/10.1002/crat.201000601.

Schopf, J. W., Farmer, J. D., Foster, I. S., Kudryavtsev, A. B., Gallardo, V. A., & Espinoza, C. (2012). Gypsum-permineralized microfossils and their relevance to the search for life on Mars. *Astrobiology*, *12*(7), 619-633. https://doi.org/10.1089/ast.2012.0827.

Shahid, S. A., & Abdelfattah, M. A. (2009). Gypsum polymorphism in the desert environment of Abu Dhabi Emirate. *European Journal of Scientific Research*, *29*(2), 237-248.

Simon, B., 1968. Contribution à l'étude de la Formation des Macles de Croissance.

Simon, B., & Bienfait, M. (1965). Structure et mécanisme de croissance du gypse. *Acta Crystallographica*, *19*(5), 750-756. https://doi.org/10.1107/S0365110X65004310.

Styles, M. T. (1996). L. L. Y. Chang, L.L.Y., Howie, R.A., Zussman, J. Rock Forming Minerals. Volume 5B: Non-silicates; sulphates, carbonates, phosphates and halides. Harlow, (Longman). ISBN 0-582-30093-2. *Mineralogical Magazine, 60*(400), 539–540. https://doi.org/10.1180/minmag.1996.060.400.20.

Sun, W., Jayaraman, S., Chen, W., Persson, K. A., & Ceder, G. (2015). Nucleation of metastable aragonite $CaCO_3$ in seawater. *Proceedings of the National Academy of Sciences*, *112*(11), 3199-3204. https://doi.org/10.1073/pnas.1423898112.

van der Voort, E., & Hartman, P. (1991). The habit of gypsum and solvent interaction. *Journal of crystal growth*, *112*(2-3), 445-450. https://doi.org/10.1016/0022-0248(91)90321-U.

Van Driessche, A. E., García-Ruiz, J. M., Delgado-López, J. M., & Sazaki, G. (2010). In situ observation of step dynamics on gypsum crystals. *Crystal growth & design*, *10*(9), 3909-3916. https://doi.org/10.1021/cg100323e

Van Driessche, A. E., García-Ruíz, J. M., Tsukamoto, K., Patino-Lopez, L. D., & Satoh, H. (2011). Ultraslow growth rates of giant gypsum crystals. *Proceedings of the National Academy of Sciences*, *108*(38), 15721-15726. https://doi.org/10.1073/pnas.1105233108

Van Driessche, A. E., Stawski, T. M., & Kellermeier, M. (2019). Calcium sulfate precipitation pathways in natural and engineered environments. *Chemical Geology*, *530*, 119274. https://doi.org/10.1016/j.chemgeo.2019.119274.

Vityk, M. O., Bodnar, R. J., & Doukhan, J. C. (2000). Synthetic fluid inclusions. XV. TEM investigation of plastic flow associated with reequilibration of fluid inclusions in natural

quartz. *Contributions to Mineralogy and Petrology*, *139*(3), 285-297. https://doi.org/10.1007/s004100000142.

Warren, J. K. (2010). Evaporites through time: Tectonic, climatic and eustatic controls in marine and nonmarine deposits. *Earth-Science Reviews*, *98*(3-4), 217-268. https://doi.org/10.1016/j.earscirev.2009.11.004.

Warren, J. K. (1982). The hydrological setting, occurrence and significance of gypsum in late Quaternary salt lakes in South Australia. *Sedimentology*, *29*(5), 609-637. https://doi.org/10.1111/j.1365-3091.1982.tb00071.x.

Weijnen, M. P. C., Van Rosmalen, G. M., Bennema, P., & Rijpkema, J. J. M. (1987). The adsorption of additives at the gypsum crystal surface: A theoretical approach: I. Determination of the interfacial bond energies. *Journal of crystal growth*, *82*(3), 509-527.https://doi.org/10.1016/0022-0248(87)90344-7.

Wenrich, K.J., Sutphin, H.B., (1994). Grand Canyon caves, breccia pipes and mineral deposits. *Geology Today, 10*(3), 97–104. Portico. https://doi.org/10.1111/j.1365-2451.1994.tb00880.x.

Wooster, W. A. (1936). On the Crystal Structure of Gypsum, $CaSO_4$ $2H_2O$. *Zeitschrift für Kristallographie-crystalline materials*, *94*(1-6), 375-396. https://doi.org/10.1524/zkri.1936.94.1.375.

Ziegenheim, S., Szabados, M., Kónya, Z., Kukovecz, Á., Pálinkó, I., & Sipos, P. (2021). Manipulating the crystallization kinetics and morphology of gypsum, $CaSO_4 \cdot 2H_2O$ via addition of citrate at high levels of supersaturation and the effect of high salinity. *Polyhedron, 204*, 115253. https://doi.org/10.1016/j.poly.2021.115253.

Appendix A

Supplementary information to chapter 1

Table S1 Some of the reference frames reported for gypsum structure. A more complete list and description can be found elsewhere in literature (Massaro et al., 2010; Aquilano et al., 2016).

a_o (Å)	b_o (Å)	c_o (Å)	β (°)	Space group	Authors
5.63	15.15	6.23	113.50	*C2/c*	de Jong and Bouman, 1939
5.67	15.201	6.274	113.91	*A2/a*	Cole and Lancucki, 1974
5.679	15.202	6.522	118.43	*I2/a*	Pedersen and Semmingsen, 1982
6.284	15.20	6.52	127.41	*C2/c*	Boeyens and Ichharam, 2002

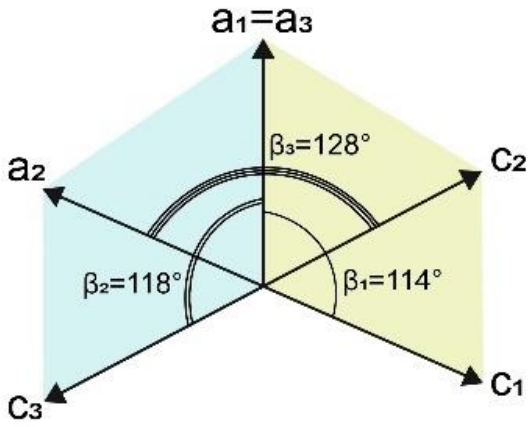

Figure S1 Plot showing how the vector choice changes in the (010) plane, according to the reference frames in Appendix A; Table S1. The [010] or the [0$\bar{1}$0] direction is perpendicular to the drawing plane (i.e., the (010)). Modified from Massaro et al., 2010.

Appendix B

Supplementary information to chapter 2

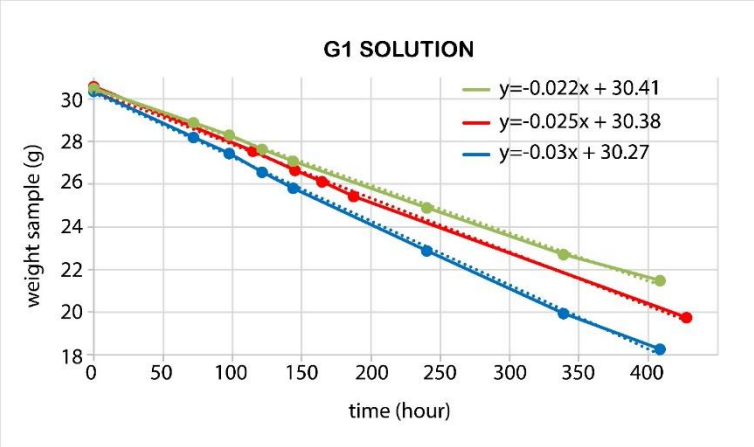

Figure S1 Evaporation rate of G1 solution.

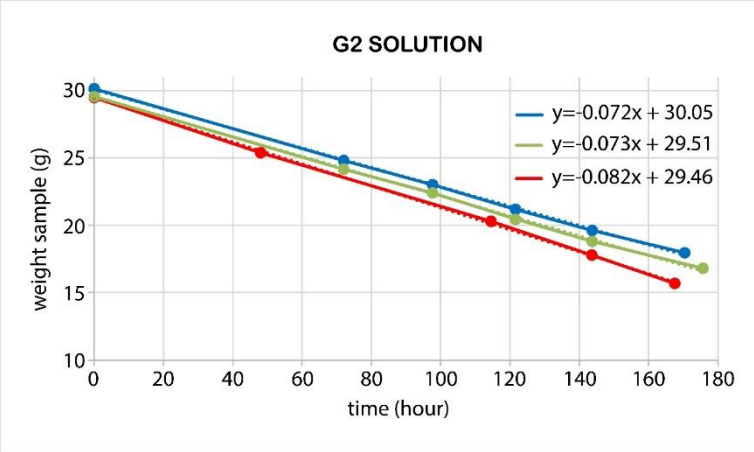

Figure S2 Evaporation rate of G2 solution.

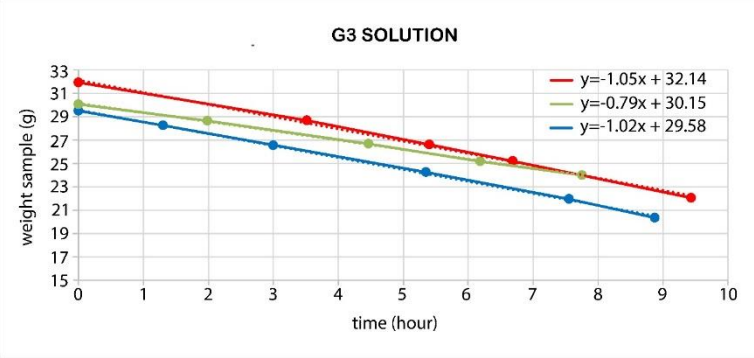

Figure S3 Evaporation rate of G3 solution.

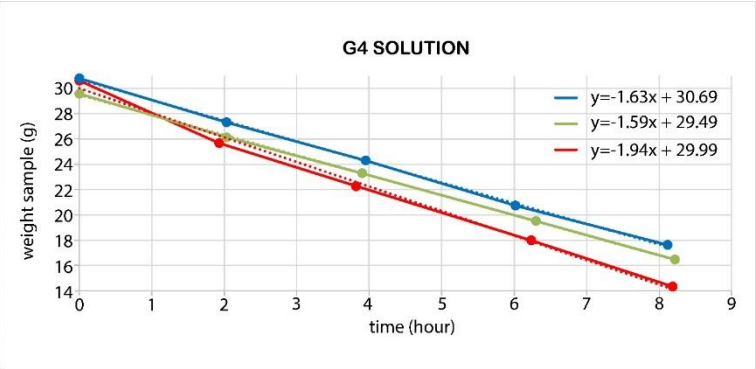

Figure S4 Evaporation rate of G4 solution.

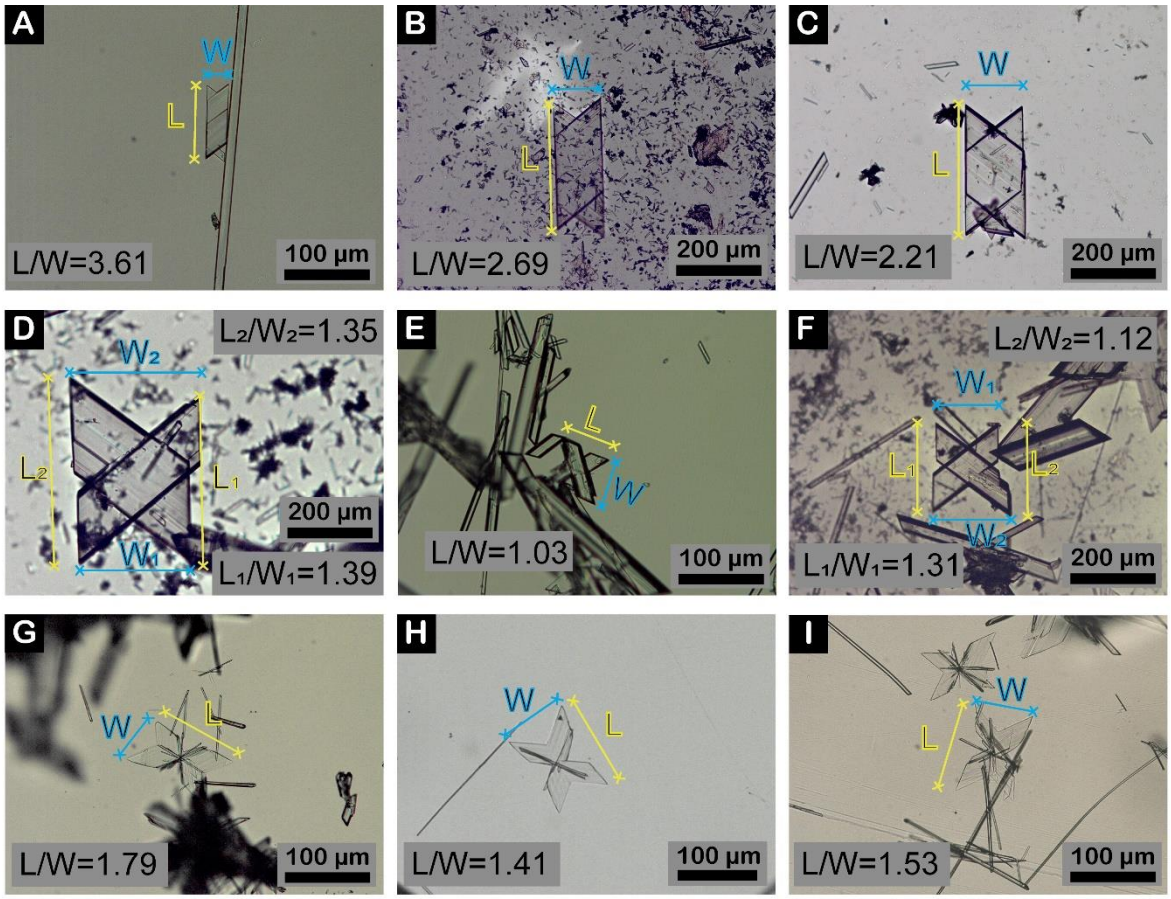

Figure S5 Aspect ratio (length-width crystal ratio) of some 100 and $\bar{1}01$ penetration twins observed in G1-G4 experiments. L=length; W=width. Only nine images of twins are reported but aspect ratio measurements have been performed on fifty different twin images, to obtain statistical information and provide reliable data (Table S1). As reported in Fig. S5-D,F, when a significance difference in the crystal aspect ratio is observed (i.e., when the length or width values between the two crystal sides differ more that 10%), both the smallest and highest length-width crystal sides are measured (L_1/W_1 and L_2/W_2 in Fig. S5-D,F, respectively; Table S1), to

provide a more complete data about aspect ratio. C) 100 penetration twins D-I) $\bar{1}01$ penetration twins.

Table S1 We have measured the aspect ratio of twenty-five of both 100 and $\bar{1}01$ penetration twins. Length and width crystal values have been measured manually with ImageJ image processing software. Each length and width measurement has been repeated three times and the average value calculated. We found a relative error less than <1% with respect to the average value in all measurements, hence the error associated to each measurement is negligible, to our purpose at least. Then, the aspect ratio has been calculated. Based on this dataset, AR of 1.97±0.01 and of 2.51±0.02 are identified as "cut off" to distinguish between 100 and $\bar{1}01$ penetration twin laws. Only 100 penetration twins show an AR>2.51±0.02, whereas only $\bar{1}01$ penetration twins have AR<1.97±0.01. In the range 1.97<AR<2.51, aspect ratio of both 100 and $\bar{1}01$ penetration twin laws have been measured and thus this range does not allow to distinguish between the two. The error associated to these values has been calculated by error propagation formula.

N°	100 penetration twin	$\bar{1}01$ penetration twin: "cruciform habit"	$\bar{1}01$ penetration twin: "butterfly habit"	L1/W1	L2/W2
1	X			3.61	–
2	X			2.69	–
3	X			2.21	–
4	X			2.41	–
5	X			2.36	–
6	X			2.20	1.98
7	X			3.15	3.79
8	X			2.88	2.68
9	X			3.25	2.56
10	X			2.68	2.12
11	X			2.42	–
12	X			3.05	2.48
13	X			2.79	2.16
14	X			2.63	3.25
15	X			3.20	2.23
16	X			3.47	2.01
17	X			3.14	2.48
18	X			2.76	–
19	X			3.02	2.82
20	X			3.87	3.53

21	X				2.94	2.87
22	X				2.58	–
23	X				1.97	2.59
24	X				2.09	2.25
25	X				4.44	3.61
26		X			1.39	1.35
27		X			1.03	–
28		X			1.31	1.12
29		X			1.33	1.04
30		X			1.39	1.27
31		X			1.73	1.19
32		X			1.14	0.90
33		X			1.74	1.26
34		X			1.12	1.04
35		X			1.20	1.12
36		X			1.58	0.84
37		X			1.31	–
38			X		1.79	–
39			X		1.41	–
40			X		1.53	–
41			X		1.25	–
42			X		1.58	–
43			X		2.13	1.67
44			X		1.51	–
45			X		–	1.32
46			X		2.51	2.04
47			X		1.43	1.12
48			X		1.79	1.27
49			X		1.59	–
50			X		1.55	1.36

Table S2 Minimum and maximum AR measured for 100 and $\overline{1}01$ penetration twins.

	Minimum value	Maximum value
100 penetration twin	1.97±0.01	4.44±0.04
$\overline{1}01$ penetration twin	0.84±0.01	2.51±0.02

The extinction angles for the five gypsum twin laws

To calculate the extinction angles of the five gypsum twin laws, it is required to:

i. Project the optical indicatrix of gypsum on the (010) plane (Fig. S2).

ii. Apply the twin law to generate the “twinned optical indicatrix” (T) (Fig. S3).

iii. Measure the angle value generated between the "old" refractive indices (e.g., γ) and the new one (γ_T or α_T) (Fig. S3). The value of this angle represents the extinction angle for the twin law, i.e., how much to rotate the crystal to move the twinned sub-crystal into extinction position when the parent sub-crystal is already extinguished.

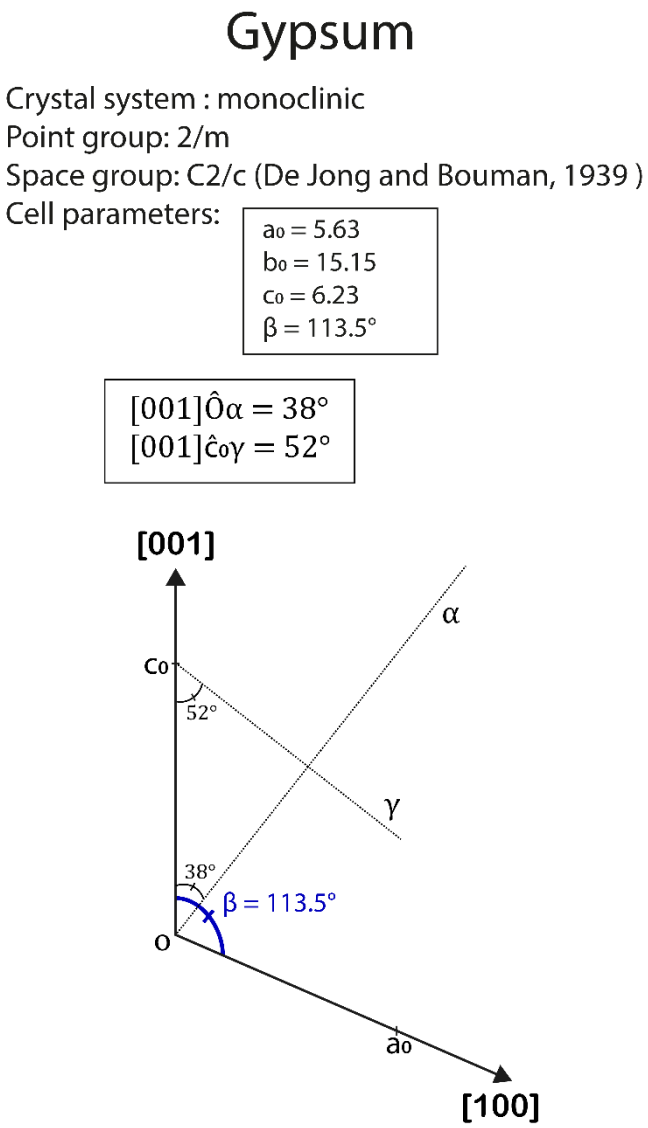

Figure S6 Gypsum reference frames used to measure the extinction angles of the five gypsum twin laws (de Jong and Bouman, 1939). α and γ represent the refractive indices of gypsum (α=1.519 – 1.521; γ=1.529 – 1.531) (Styles et al., 1996). The monoclinic *C2/c* space group of gypsum ($a_0 = 5.63,\ b_0 = 15.15,\ c_0 = 6.23$ Å; $\alpha = \gamma = 90°;\ \beta = 113.50°$) (de Jong and Bouman, 1939) has been used to project the optical indicatrix of gypsum on the (010) plane.

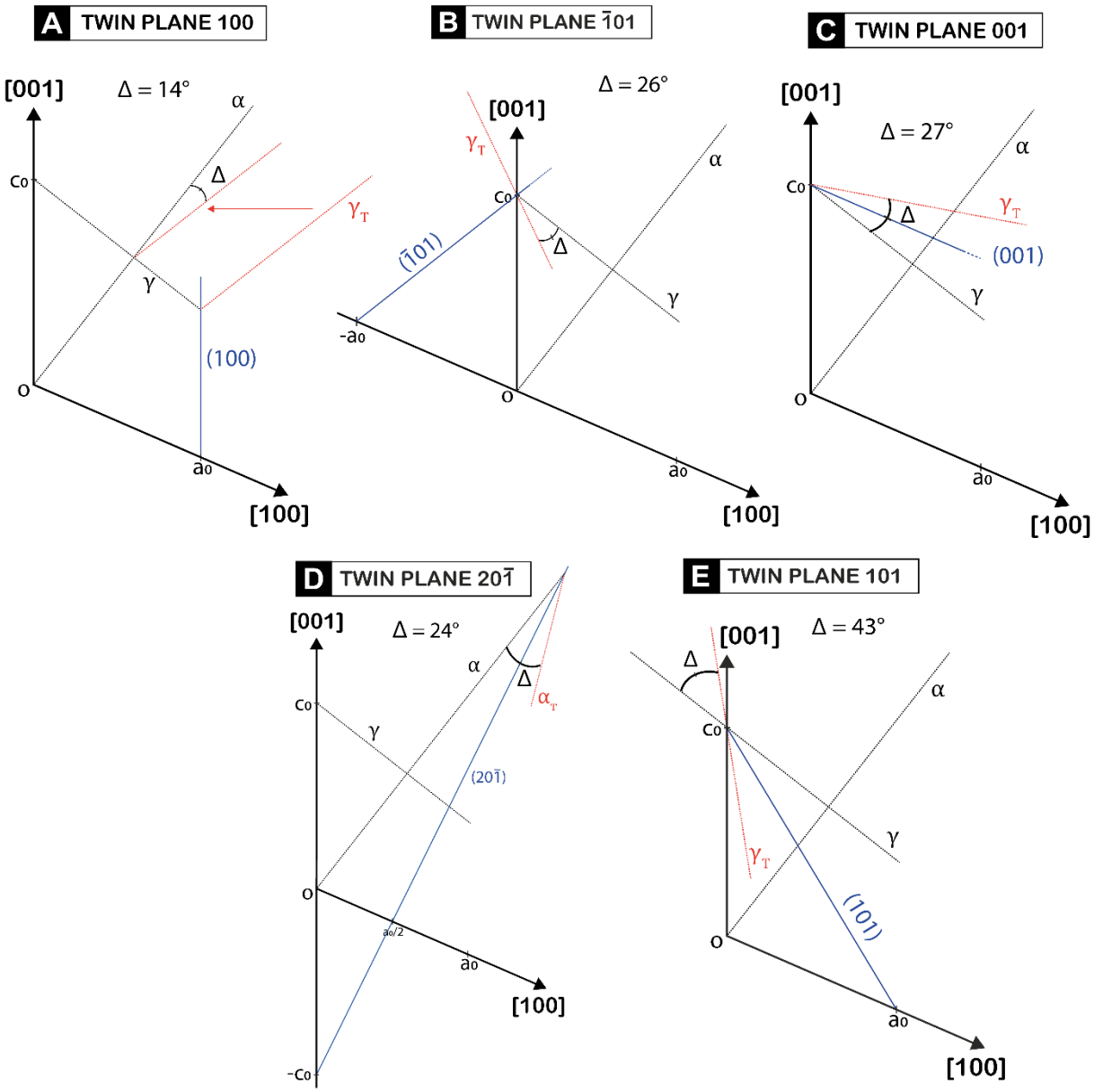

Figure S7 Extinction angles of the five gypsum twin laws.

Appendix C

Supplementary information to chapter 3

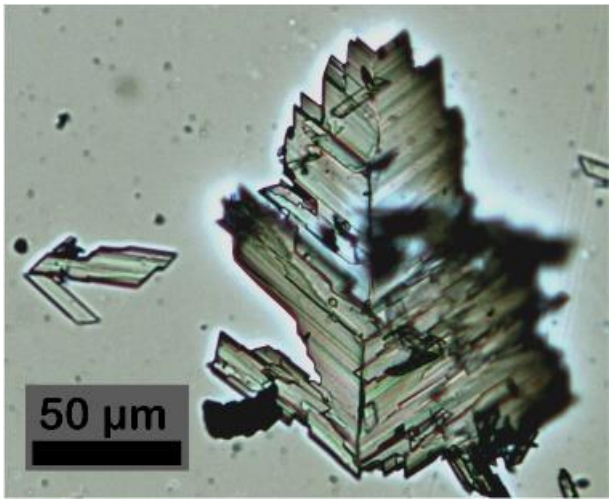

Figure S1 Optical microscopy image of $\bar{1}01$ contact twin observed in G2 solution. By means optical microscopy under crossed polarizers we measured 26° as extinction angle among the individuals forming the twin, and thus, we identified the $\bar{1}01$ twin law.

Appendix D

Supplementary material to chapter 4

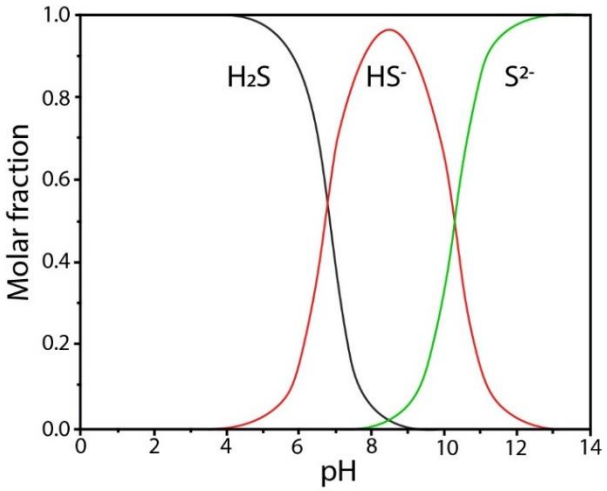

Figure S1 Acid dissociation of H_2S in water: pK1=7.0; pK2=12.9.

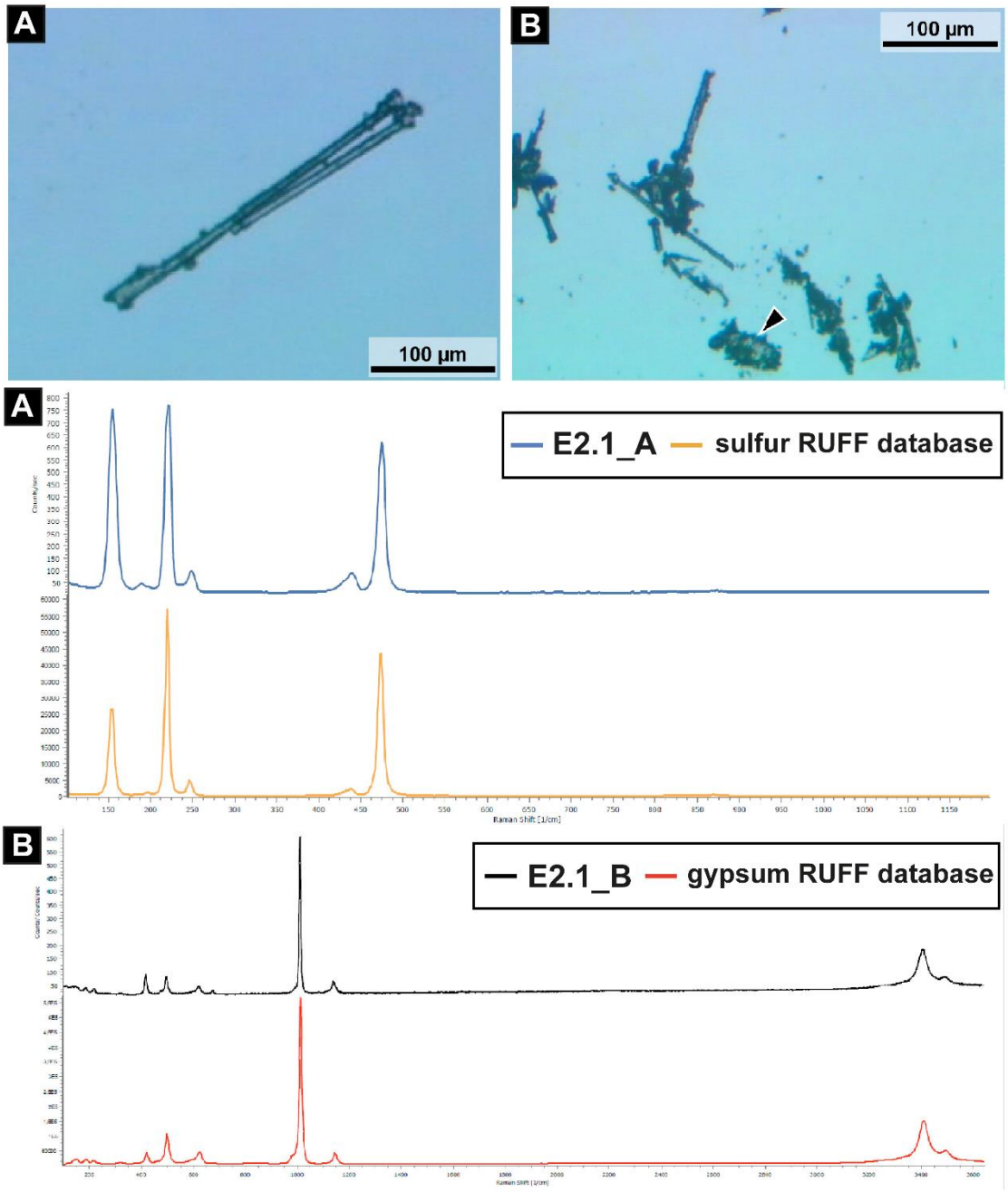

Figure S2 µ-Raman analysis was performed on the solid fraction of E2 (i.e., E2.1). A) Optical microscope image of a rod-shaped crystal and the associated Raman spectrum. The Raman spectrum of the crystal (A) is in perfect agreement with that one obtained from the Raman database for minerals (RRUFF database). B) Optical microscope image of aggregate crystals and related Raman spectrum. The Raman spectrum (B) perfectly agrees with the gypsum spectra of the RRUFF database.

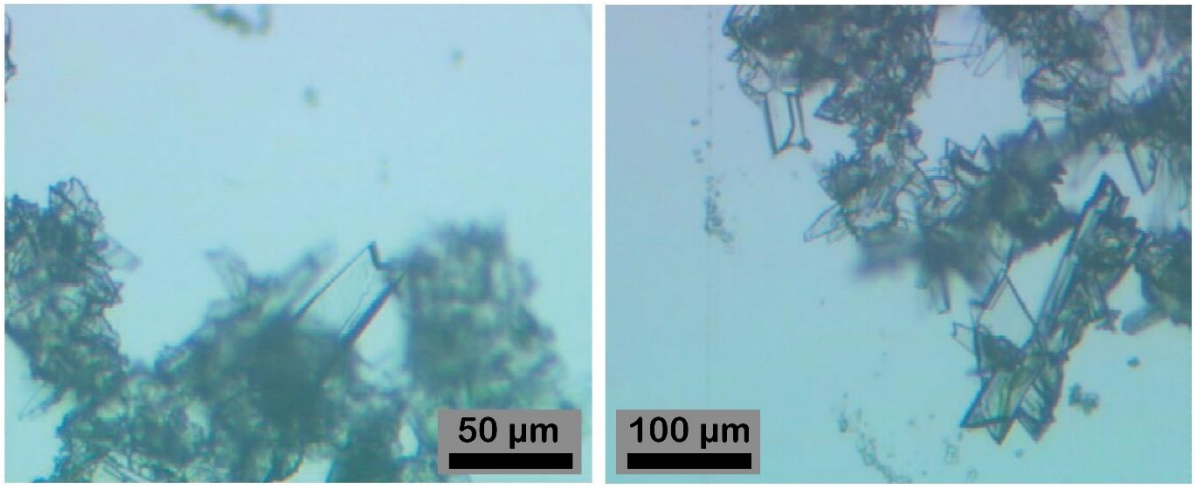

Figure S3 Optical microscopy image of gypsum twins observed in E2.2 solution. By means optical microscopy under crossed polarizers we measured 14° as extinction angle among the individuals forming the twin, and thus, we identified the 100 twin law.